GLOBAL STRATIGRAPHY OF VENUS: ANALYSIS OF A RANDOM SAMPLE OF THIRTY-SIX TEST AREAS

ALEXANDER T. BASILEVSKY[1,2] and JAMES W. HEAD, III[1]
[1]*Department of Geological Sciences, Brown University, Providence, Rhode Island;* [2]*Vernadsky Institute of Geochemistry and Analytical Chemistry, Russian Academy of Sciences, Moscow, Russia*

(Received 29 November 1994)

Abstract. The age relations between 36 impact craters with dark paraboloids and other geologic units and structures at these localities have been studied through photogeologic analysis of Magellan SAR images of the surface of Venus. Geologic settings in all 36 sites, about 1000 × 1000 km each, could be characterized using only 10 different terrain units and six types of structures. These units and structures form a major stratigraphic and geologic sequence (from oldest to youngest): 1) tessera terrain; 2) densely fractured terrains associated with coronae and in the form of remnants among plains; 3) fractured and ridged plains and ridge belts; 4) plains with wrinkle ridges; 5) ridges associated with coronae annulae and ridges of arachnoid annulae which are contemporary with wrinkle ridges of the ridged plains; 6) smooth and lobate plains; 7) fractures of coronae annulae, and fractures not related to coronae annulae, which disrupt ridged and smooth plains; 8) rift-associated fractures; 9) craters with associated dark paraboloids, which represent the youngest 10% of the Venus impact crater population (Campbell *et al.*, 1992), and are on top of all volcanic and tectonic units except the youngest episodes of rift-associated fracturing and volcanism; surficial streaks and patches are approximately contemporary with dark-paraboloid craters.

Mapping of such units and structures in 36 randomly distributed large regions (each $\sim 10^6$ km^2) shows evidence for a distinctive regional and global stratigraphic and geologic sequence. On the basis of this sequence we have developed a model that illustrates several major themes in the history of Venus. Most of the history of Venus (that of its first 80% or so) is not preserved in the surface geomorphological record. The major deformation associated with tessera formation in the period sometime between 0.5–1.0 b.y. ago (Ivanov and Basilevsky, 1993) is the earliest event detected. In the terminal stages of tessera formation, extensive parallel linear graben swarms representing a change in the style of deformation from shortening to extension were formed on the tessera and on some volcanic plains that were emplaced just after (and perhaps also during the latter stages of the major compressional phase of tessera emplacement. Our stratigraphic analyses suggest that following tessera formation, extensive volcanic flooding resurfaced at least 85% of the planet in the form of the presently-ridged and fractured plains. Several lines of evidence favor a high flux in the post-tessera period but we have no independent evidence for the absolute duration of ridged plains emplacement. During this time, the net state of stress in the lithosphere apparently changed from extensional to compressional, first in the form of extensive ridge belt development, followed by the formation of extensive wrinkle ridges on the flow units. Subsequently, there occurred local emplacement of smooth and lobate plains units which are presently essentially undeformed. The major events in the latest 10% of the presently preserved history of Venus (less than 50 m.y. ago) are continued rifting and some associated volcanism, and the redistribution of eolian material largely derived from impact crater deposits.

Detailed geologic mapping and stratigraphic synthesis are necessary to test this sequence and to address many of the outstanding problems raised by this analysis. For example, we are uncertain whether this stratigraphic sequence corresponds to geologic events which were generally synchronous in all the sites and all around the planet, or whether the sequence is simply a typical sequence of events which occurred in different places at different times. In addition, it is currently unknown whether the present state represents a normal consequence of the general thermal evolution of Venus (and is thus representative of the level of geological activity predicted for the future), or if Venus, has been characterized by a sequence of periodic global changes in the composition and thermal state of its crust and upper mantle (in which case, Venus could in the future return to levels of deformation and resurfacing typical of the period of tessera formation).

Earth, Moon and Planets **66:** 285–336, 1995.

1. Introduction

High-resolution global Magellan images of Venus provide an opportunity to analyze the stratigraphic relationships among various structures and terrains on Venus. This is a necessary step in order to work out a reliable scenario for the geologic history of this planet and compare it with geologic histories of other planets, especially with Earth's. Our goal is to examine a series of randomly distributed regions on Venus to work out a sequence of stratigraphic events in each region, and then to discern if there are any general themes within and between these areas that might provide insight into Venus global stratigraphy. This approach will help to consider the results of ongoing geological quadrangle mapping in a broad regional and even global context; such systematic mapping is now in progress as part of the Venus Data Analysis Mapping Program (VMAP) and one of the major goals is the development of a global geologic history. Indeed, this systematic mapping will test and modify our initial general findings.

Our approach is similar to that commonly used in photogeologic stratigraphy (e.g., Wilhelms, 1972, 1990). On Earth, rock-stratigraphic units are defined as "... a subdivision of the rocks in the Earth's crust distinguished and delimited on the basis of ... observable physical features ... [commonly lithologic] ... and independent from time concepts ... and ... inferred geologic history..." (ACSN, 1961). In planetary mapping stratigraphic units must be defined largely by remote sensing and so it is difficult to approach the process of geologic mapping of planetary crusts with a strict 'lithologic' definition of units (Head *et al.*, 1978). As outlined by Wilhelms (1972, 1990), planetary mappers use the broader definition of rock-stratigraphic units as those "distinguished and delimited on the basis of observable physical features", which might include surface morphology, albedo, etc. (see also Head *et al.*, 1978).

Published global geologic maps for the planet Mars at a scale of 1:15 million (Scott and Tanaka, 1986; Tanaka and Scott, 1987; Greeley and Guest, 1987) provide some perspective and precedent for unit definition and characterization on Venus. First, in terms of description of map units (Scott and Tanaka, 1986), "although the origin and composition of many units are obscure or controversial, their interpretations are based on objective descriptions of morphologic characteristics visible on ... photomosaics and images". In addition to surface roughness and albedo, a wide range of morphologic structures and textures is utilized to define, distinguish, and characterize units, including crater densities, tectonic fractures, flow lobes, channels, eolian pits, tectonic ridges, and mountain ranges such as crater and basin rims. For example, the Grooved member of the Vastitas Borealis Formation is defined by "curvilinear and polygonal patterns of grooves and troughs", while the Ridged member is characterized by a "concentric pattern of low, narrow ridges about 1 to 2 km wide". Member 6 of the Tharsis Montes Formation is defined by "fresh-appearing lava flows (that) form smooth fan-shaped arrays". The four Aureole members of the Olympus Mons Formation are defined as "broad,

semicircular, flat lobes; corrugated, cut by numerous faults that formed scarps and deep troughs and grabens". Crater density and intensity of structural deformation are used in distinguishing units as in the case of the Lower member of the Syria Planum Formation, which is defined as being "similar to the upper member but more highly cratered and faulted". Erosional landforms are used in unit definition in the Plateau Sequence, where the Dissected unit is "similar in appearance to the cratered unit but more highly dissected by small channels and troughs", the Etched unit is "deeply furrowed by sinuous, intersecting curved to flat-bottom grooves that produce an etched or sculptured surface", and the Ridged unit is defined by "long, linear to sinuous mare-type (wrinkle) ridges". Finally, structural deformation plays a large role in the definition of a major geologic unit known as Highly Deformed Terrain Materials, where "the origin and composition of these rock units are only surmised because multiple sets of fractures and grabens have obscured original characteristics". Subunits include Younger Fractured Material, which forms "relatively smooth raised surfaces of moderate relief with fractures, grabens, and collapse depressions", Older Fractured Material, which "is more highly deformed and faults are more complexly oriented", and a Basement Complex, which is "undifferentiated material characterized by highly complicated structure and prominent relief".

In addition to morphologic features and structures forming an integral part of the definition of geologic map units on Mars, such large or prominent features (faults, graben, wrinkle ridges, sinuous channels, depressions, etc.) are sometimes mapped individually at this scale (e.g., Scott and Tanaka, 1986). Indeed, the distinction and individual mapping of such features, or their inclusion in the definition of a unit, is clearly a function of the scale of mapping. What might be mapped separately as individual structures at a scale of 1:100,000, would very likely be included as part of a unit definition or characterization at a scale of 1:15 M.

On the basis of these descriptions and the utilization of surface morphology and tectonic structure, these units might be better described as morphostratigraphic units, rather than narrowly defined rock units. Nonetheless they form a consistent basis on which to subdivide the crust of Mars into map units which can be used to establish correlations, interpret the geologic processes operating during their formation and modification, and to interpet the geologic history of Mars (Scott and Tanaka, 1986; Tanaka and Scott, 1987; Greeley and Guest, 1987).

In this paper we have employed a range of observable physical features that are commonly used on other planets and that are also related to the characteristics of the remote sensing instrument and wavelengths of the data [e.g., morphologic patterns, regional smoothness or roughness, radar brightness patterns at the scale of the radar (surface roughness at the rock/soil scale), structure, etc.]. We follow the U.S. Geological Survey "Venus Geologic Mappers' Handbook" (Tanaka, 1994) in which "Map units will be defined on the basis of various morphologic, textural, and structural characteristics observable in Magellan images."

Although we have mapped tectonic structure independent of geologic units, as in the case of fractures (F), in many cases tectonic features are such a pervasive part of the morphology of the terrain that it becomes part of the definition of a unit, as in the Mars examples cited above. For example, our tessera unit is similar to several members of the Olympus Mons Formation (Aureole members 1–4) which are defined on the basis of tectonic structure ("... corrugated, cut by numerous faults that formed scarps and deep troughs and grabens...", Scott and Tanaka, 1986). Our plains with wrinkle ridges unit is analogous to Member 1 of the Arcadia Formation on Mars ("Low-lying plains; mare-type (wrinkle) ridges common"). In other cases, we do both depending on scale and density. For example, in the case of Rift-associated fractures (Fra), when the structures are more discrete and separated, we map them separately and not as a specific unit (for example, Figure 8), while in other cases, where they are very dense and tend to obscure the underlying terrain, one may map them as a unit (for example, Figures 13-15).

In this analysis we use a specific stratigraphic marker to choose the areas of analysis. This marker is the presence of dark paraboloid craters which are considered to be among the youngest 10% of the Venus crater population (Campbell *et al.*, 1992); this means that they are evidently younger than about 30–50 m.y. (Basilevsky, 1993; Strom, 1993). The presence of these features in the areas of study provides an opportunity to check whether or not there are other very young geologic formations at the sites. This is important as a test of the idea that most of the presently observed features and terrains on Venus were formed rather early as a result of a cataclysm about 300–500 m.y. ago and following this only minor geologic activity occurred (Schaber *et al.*, 1992; Strom *et al.*, 1994).

Moreover, due to the nature of impact cratering the position of the youngest impact craters should be random and thus independent of local volcanic and tectonic geology. So, using the presence of the dark paraboloid craters as a criterion for the selection of the sites we avoid a possible bias in preference or neglect of geologic formations due to investigator bias. Following this approach we selected as the centers of our study areas 36 craters with dark paraboloids of the so-called pd-type (filled-in parabola). These 36 craters (Figure 1) are all the craters of this type listed by Campbell *et al.*, 1992. At our request, E. V. Zabalueva, a mathematician at the Vernadsky Institute, made three statistical tests to check whether the distribution of those 36 craters over Venus is random. The tests were the same as those used by Phillips *et al.* (1992) in their study of the impact crater populations of Venus (Diggle *et al.*, 1985). All three tests (Rayleigh, Gine, and "small angles") showed that the distribution of these 36 craters on the Venus globe is indistinguishable from a random one.

In the present study we have analyzed the age relations among 36 impact craters with dark paraboloids and other geologic formations and structures at these localities. Specifically, we are trying to find what geologic phenomena occurred in these regions prior to and after the formation of the craters. For each of these sites we have analyzed the stratigraphic relationships among all major features,

structures, and terrains within the areas of about 1,000 × 1,000 km centered at the craters. The detailed description of these features and their relationships is contained in Basilevsky and Head (1994) and is summarized in the following discussion and geologic sketch maps. We made this analysis using both 20 × 24″ hard copies of the appropriate F-MIDRPs and C1-MIDRPs as well as CDROM digital data (altimetry and images) for key areas of the sites. The total area of the 36 sites is about 36×10^6 km^2, about 8% of the total surface of Venus. Of course, using the approach of random sampling we may have some unsampled geologic formations and our conclusions about the global stratigraphy of Venus might be incomplete. For example, we have not sampled in our sites the mountain ranges of Akna, Frejya and Maxwell Montes.

2. Features, Structures, and Units Used in Local Analyses

The list of sites under study is given in Table I and their locations are shown on Figure 1. In the description of all 36 sites we could characterize practically all geologic situations using only 16 major types of terrain units and structures, and typical examples of these and their locations are shown in Figure 2 and Table II. Units and structures are designated by letters for ease of discussion and mapping. In cases where structures are very common, a line is drawn around them and their presence is indicated by the letter designation. A sketch map of a hypothetical area showing the typical distribution and configuration of units and structures, and a legend for this and subsequent maps, is shown in Figure 3a. The units and structures include:

1) *Tessera (Tt)*: This geologic unit consists of at least two sets of intersecting ridges and grooves, and is a result of tectonic deformation of some precursor terrain (Barsukov *et al.*, 1986; Basilevsky *et al.*, 1986; Bindschadler and Head, 1991; Sukhanov, 1992; sometimes referred to as complex ridged terrain, Solomon *et al.*, 1992). Typical spacing for tessera topographic features is about 10 km with variations from 5 to 20 km. This wavelength is usually complicated by faults with spacing of about 1 km (Figure 2, Section 1). Tessera ridges and grooves are tectonic features, so structure is an essential component of the tessera terrain and a key aspect of the unit definition. The untectonized tessera precursor terrain was not observed. Tessera forms continental-like blocks and small islands standing above and embayed by adjacent plains. Tessera occupies about 8% of the surface of Venus (Ivanov and Head, 1994) and was observed in 23 of the 36 sites studied.

2–3) *Densely fractured terrain*: These units consist of swarms of subparallel and sometimes of intersecting or radial fractures with typical spacing of about 1 km or less (Figure 2, Sections 2, 3). The unmodified precursor terrain for the densely fractured terrains was not observed. Apparently it was plains because if we ignore the fractures the terrain looks quite smooth (Figure 2, Section 3). Two varieties of this terrain are distinguished: 2) densely fractured terrain of coronae (COdf) which

TABLE I

Location of the 36 dark paraboloid (pd type; Campbell *et al.*, 1992) crater sites used for stratigraphic analysis in this study

Number	Crater	Latitude, °N	Longitude, °E	Diameter, km
1	Annia Faustina	22.09	4.69	22.0
2	Holiday	−46.73	12.83	26.0
3	Ruth	43.30	19.84	18.0
4	Stuart	−30.77	20.23	67.0
5	Noreen	33.58	22.69	18.2
6	Bathsheba	−15.04	49.44	36.0
7	Francesca	−28.00	57.80	18.0
8	Bassi	−18.95	64.71	35.0
9	Jadwiga	68.40	91.01	12.0
10	Li-Quingzhao	23.74	94.62	21.0
11	Boulanger	−26.61	99.25	57.0
12	Caldwell	23.57	112.34	48.0
13	Yonge	−13.96	115.06	28.0
14	Merit-Ptah	11.39	115.65	20.0
15	Pimiko	19.02	124.22	35.0
16	Phyllis	12.37	132.38	13.0
17	Greenaway	22.92	145.12	89.0
18	Ban-Zhao	17.17	146.96	36.0
19	Austen	−24.98	168.38	45.0
20	Martinez	−11.64	174.75	24.0
21	Akiko	30.66	187.25	22.0
22	Yablochkina	48.28	195.30	55.0
23	Uvaysi	2.37	198.24	40.0
24	Edinger	−68.80	208.42	35.0
25	Boleyn	24.42	220.05	65.0
26	Akeley	8.01	244.53	25.0
27	Glaspell	−58.42	269.51	25.0
28	Lyon	−66.49	270.54	12.5
29	Montessori	59.43	279.92	42.0
30	Cotton	70.77	300.17	45.0
31	Dashkova	78.24	306.25	50.0
32	Aurelia	20.27	331.80	31.0
33	Magnani	58.63	337.19	26.6
34	Comnena	1.17	343.72	20.0
35	Carson	−24.17	344.12	39.0
36	Audrey	23.77	348.11	15.0

Table II. Location of the typical examples of the 16 major types of units and structures (S) (see Figure 2) encountered in mapping in 36 areas

N	Unit	Symbol	Site Number	Area size, km	Coordinates of the Center	Image Source
1	Tessera	Tt	8	50 × 50	9.3°S, 62.5°	F-MIDRP.10S065;1
2	Densely fractured terrain of coronae	COdf	30	50 × 50	68.2°N, 295.4°	F-MIDRP.70N296;1
3	Densely fractured terrain of the plains	Pdf	1	50 × 50	19.2°N, 3.6°	F-MIDRP.20N003;1
4	Fractured & ridged plains	Pfr	21	50 × 50	35.6°N, 195.9°	F-MIDRP.35N197;1
5	Ridge belts (S)	RB	2	80 × 80	39.9°S, 18.7°	C1-MIDRP.45S011;1
6	Plains with wrinkle ridges	Pwr	22	50 × 50	38.8°N, 196.9°	F-MIDRP.40N194;1
7	Ridges of corona annulus (S)	COar	29	50 × 50	56.1°N, 295.9°	F-MIDRP.55N291;1
8	Ridges of arachnoid annulus (S)	Aar	3	50 × 50	45.2°N, 19.2°	F-MIDRP.45N019;1
9	Smooth plains	Ps	2	50 × 50	52.1°S, 14.5°	F-MIDRP.50S013;1
10	Lobate plains	Pl	36	50 × 50	18.3°N, 348.5°	F-MIDRP.20N351;1
11	Fractures of corona annulus (S)	COaf	19	50 × 50	25.1°S, 174.0°	F-MIDRP.25S174;1
12	Fractures (S)	F	2	50 × 50	50.3°S, 17.5°	F-MIDRP.50S013;1
13	Rift-associated fractures (S)	Fra	1	50 × 50	18.2°N, 1.6°	F-MIDRP.20N003;1
14	Craters with dark paraboloids	Cdp	6	1000 × 1000	15.0°S, 46.5°	C2-MIDRP.30S026.201
15	Surficial streaks	Ss	29	50 × 50	59.0°N, 279.3°	F-MIDRP.60N281;1
16	Surficial patches	Sp	29	50 × 50	57.8°N, 270.0°	F-MIDRP.60N270;1

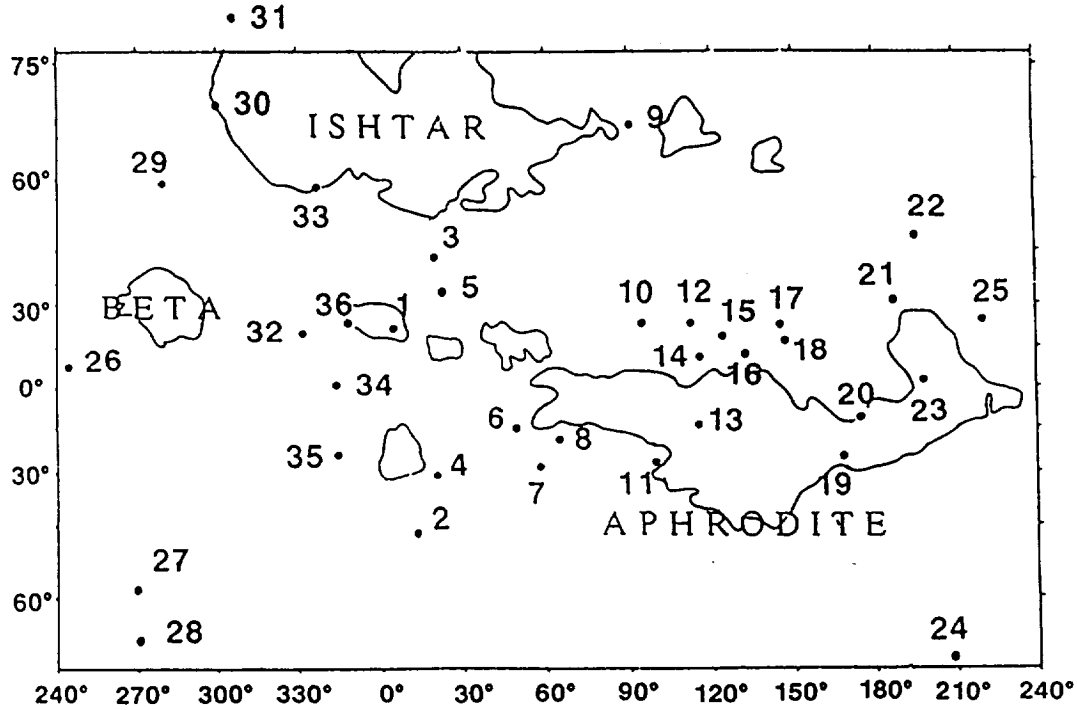

Fig. 1. Global distribution of the 36 sites containing craters with dark paraboloids that were analyzed in this study. Major highland areas are outlined. The coordinates of each site are listed in Table I.

is usually with radial or chaotic intersecting patterns (Figure 2, Section 2), and 3) densely fractured terrain which forms remnants among the plains (Pdf) not being part of identified coronae; its pattern of fracturing is usually subparallel (Figure 2, Section 3). Although fractures are structural elements, they are such a pervasive part of the morphology of this terrain that it becomes a key aspect of the definition of the unit, as in several of the Mars examples cited above. Pdf was observed in thirty-three of the 36 sites and COdf was observed in twenty of the 36 sites. In 18 sites both Pdf and COdf are present and the average percentage of area occupied by Pdf/COdf is estimated to be 3–5%.

4) *Fractured and ridged plains (Pfr)*: This terrain is present in the form of remnants usually among plains with wrinkle ridges. A typical characteristic of Pfr is the presence of relatively broad (5–10 km wide) ridges tens of km long, usually arranged *en echelon* and forming belts (Figure 2, Section 4). Besides the ridges, Pfr has fractures at least part of which predated the ridges. In some cases these fractures are evidently a remnant of Pdf inside Pfr. Fractures and ridges are structural elements, but at this scale they are a basic part of the morphology of this terrain and thus become an important aspect of the definition of the unit. If one were mapping at a large scale a small area within this unit, one might map the fractures and ridges individually. Pfr was observed in six of the 36 sites. If averaged for all the sampled surface, Pfr occupies no more than 1–3% of the surface.

5) *Ridge belts (RB)*: This structure (Figure 2, Section 5) was observed in prominent form in the sampled sites only one time (site #2). The ridge belt there consists

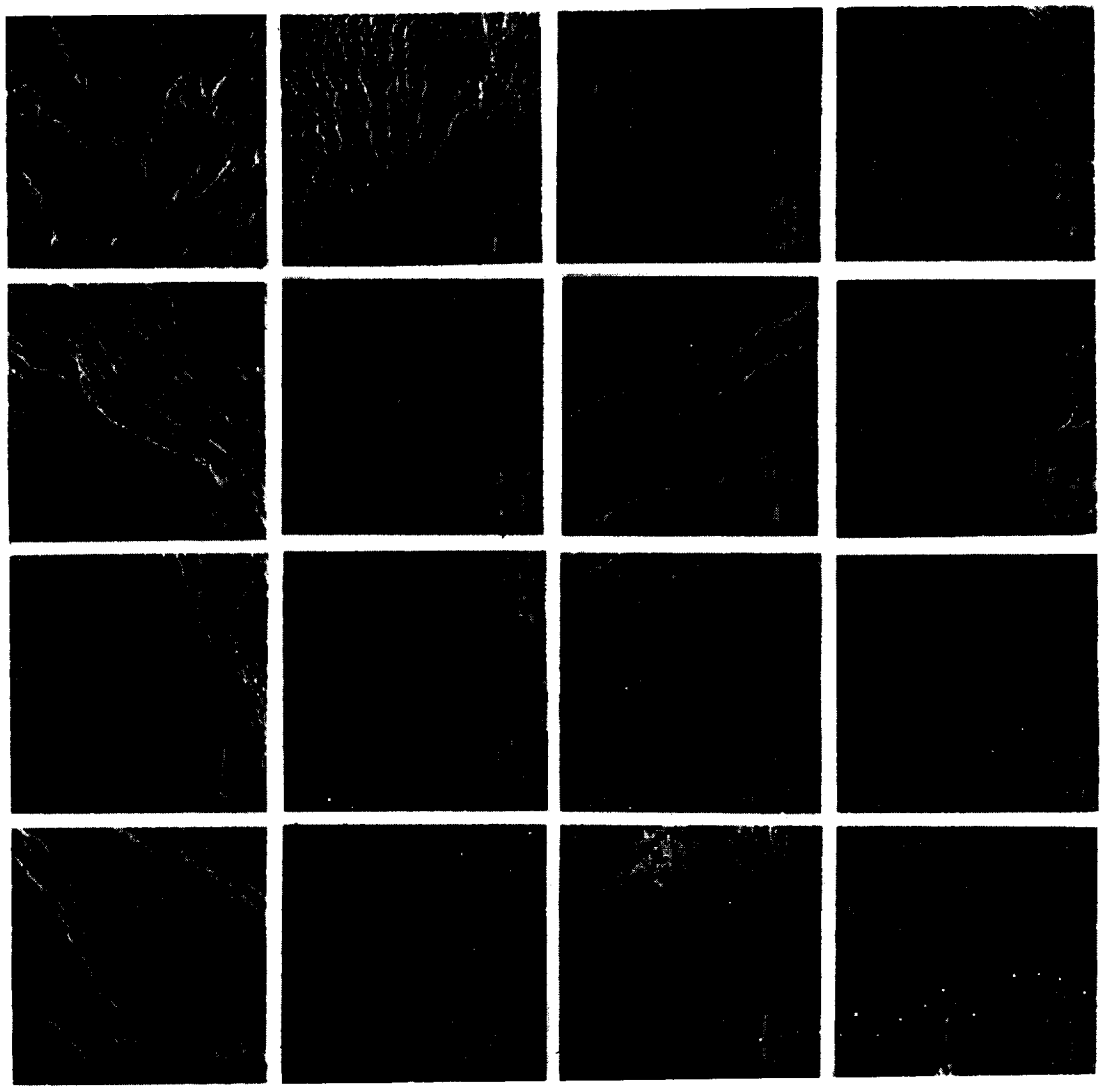

Fig. 2. Examples of the 16 different units and structures distinguished and mapped in this study. The width of each example is 50 km, with the exception of number 14, which is 1000 km. 1) Tessera (unit Tt); 2) Densely fractured terrains associated with coronae (unit COdf), and 3) in the form of remnants among plains (unit Pdf); 4) Fractured and ridged plains (unit Pfr); 5) Ridge belts (RB structure); 6) Plains with wrinkle ridges (unit Pwr); 7) Ridges associated with coronae annulae (COar structure); 8) Ridges of arachnoid annulae (Aar structure); 9) Smooth plains (unit Ps); 10) Lobate plains (unit Pl); 11) Fractures of coronae annulae (COaf structure); 12) Fractures (F structure); 13) Rift-associated fractures (Fra structure); 14) Craters with associated dark paraboloids (unit Cdp); 15) Surficial streaks (unit Ss); 16) Surficial patches (unit Sp). The locations of each of these typical areas listed in Table II and the unit and structural map designations are shown in Figure 3a.

of a cluster of densely spaced ridges of 5 to 10 km width and a few tens of km long. In some places there are plains areas among the ridges and the terrain resembles fractured and ridged plains (Pfr). In less prominent form, ridge belts are also seen in site #24.

6) *Plains with wrinkle ridges (Pwr)*: This is the most abundant terrain composing in most cases a background on which many other features and terrains are seen.

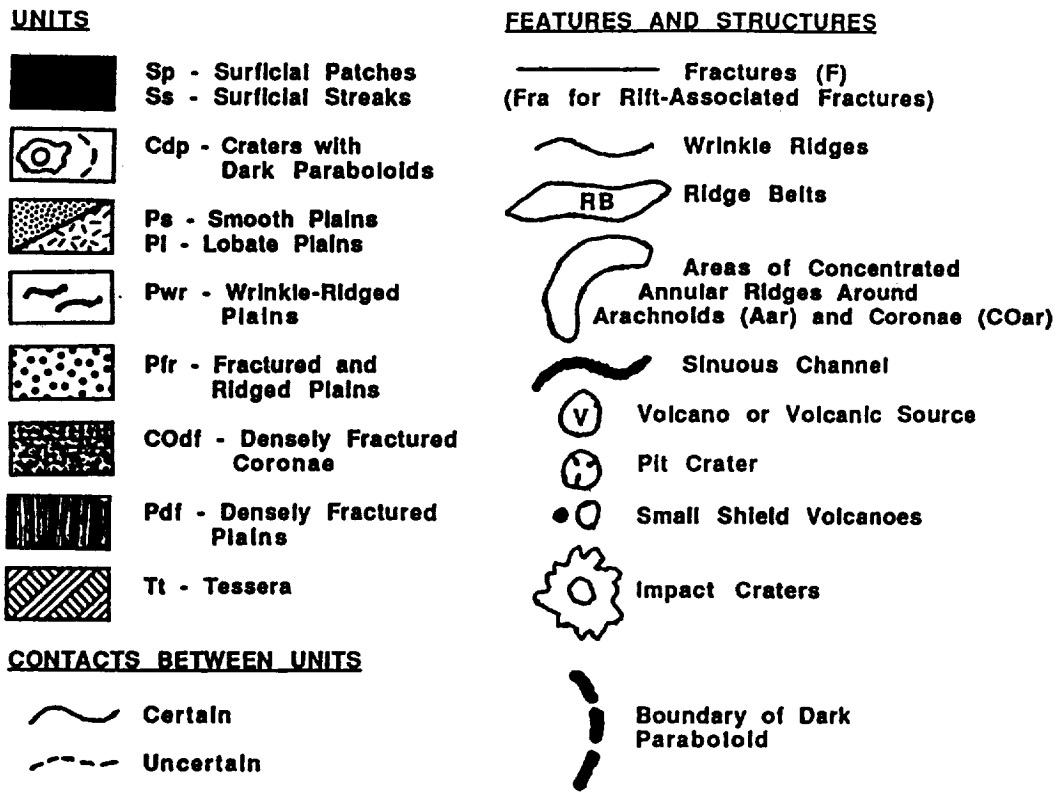

Fig. 3a.

Fig. 3. a) Legend for the geological sketch maps shown in Figures 3b–15. b) Geologic sketch map of a hypothetical area showing the typical distribution and characteristics of the major units and structures found in the 36 mapped areas. An ancient tessera unit (Tt) is embayed by densely fractured plains (Pdf) which in turn are embayed by plains with wrinkle ridges (Pwr). The general trends of individual wrinkle ridges are shown by wavy lines. These are flooded and embayed by smooth plains (Ps) and lobate plains (Pl). In the northwest part of the area, the plains are cut by rift-associated fractures (Fra; mapped here as individual fractures) which are disrupted by the formation of a dark paraboloid crater (Cdp), the floor of which is cut by post-crater-formation rift-associated fractures. This indicates that rift-associated fractures are continuing to form throughout the latter stages of the history of this region. Surficial material, most likely from the crater ejecta, has been mobilized to form streaks (Ss). The map unit and structure designations shown in the legend are those used for the individual mapped areas, a selection of which is shown in Figures 4–15. This sketch map also illustrates the types of relationships used to establish stratigraphy and relative sequence of events at each site such as embayment relationships (A), cross-cutting relationships (B), and superposition relationships (C).

Pwr is usually radar dark or moderately dark. However, in some areas, it has quite bright subunits which may have lava flow-like morphology. A typical characteristic of Pwr is the presence of a network of wrinkle ridges which is a structural element (Figure 2, Section 6). The ridges usually are less than 1 km wide and a few tens of km long; in some areas they may be smaller while in others they are larger. Their trend often varies even within one site. This unit is analogous to the previously mentioned Ridged unit of the Plateau Sequence on Mars (Scott and Tanaka, 1986) which is a plains unit defined by "long, linear to sinuous mare-type (wrinkle)

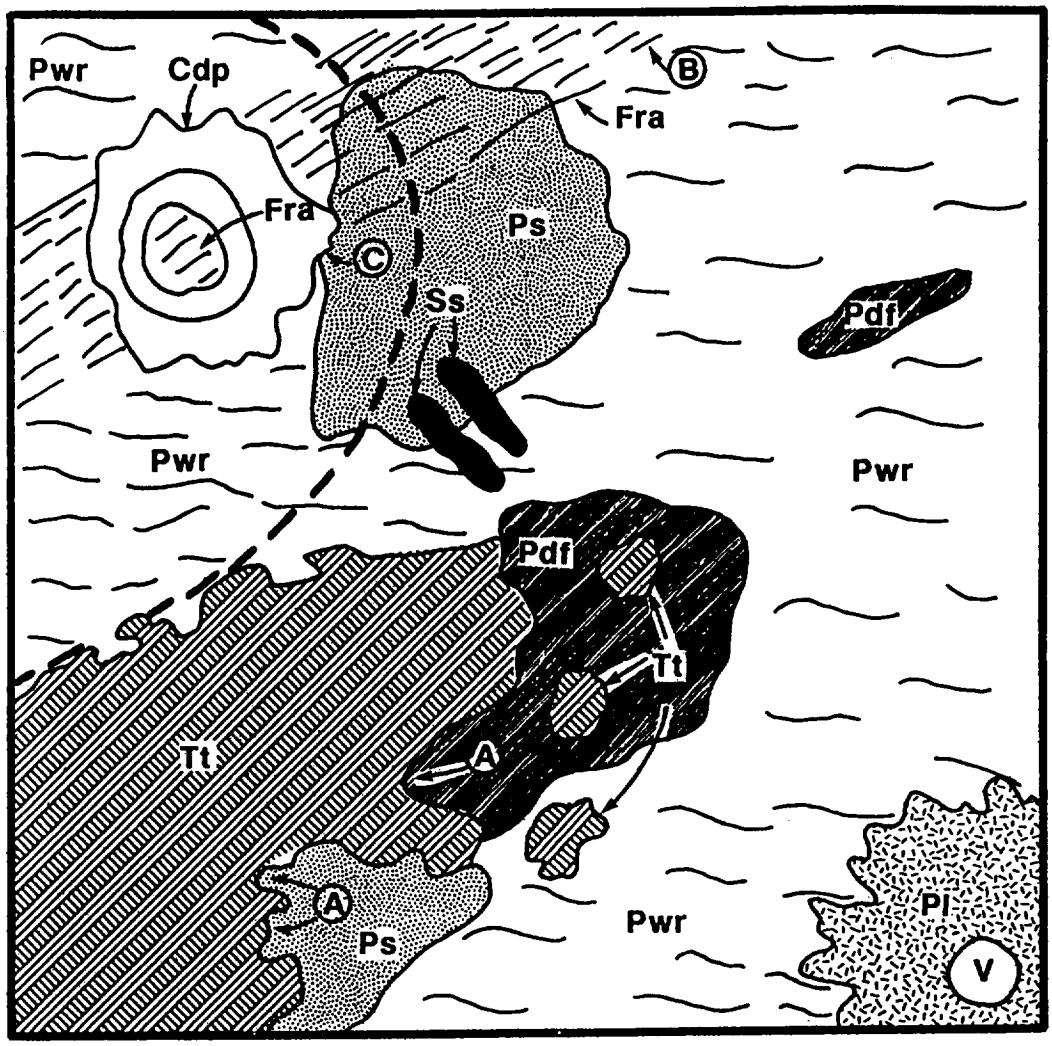

Fig. 3b.

ridges". Pwr was observed in all 36 sites. Their abundance is estimated to be about 70% of the surface of Venus.

7) *Ridges of corona annulus (COar)*: These structures (Figure 2, Section 7) outline annuli of many coronae. As a rule they consist of an outline of sectors of an incomplete circle. COar were observed in 13 of the 36 sites. In 12 sites they are in structural alignment with wrinkle ridges, and this implies that they were formed contemporaneously. In one site (#26) their stratigraphic position is not clear; they may postdate plains with wrinkle ridges or may be contemporaneous with wrinkle ridges. COar usually is more prominent than the neighboring wrinkle ridges. The width of these ridges is, as a rule, 2 to 3 km and sometimes they reach 5–8 km while the wrinkle ridges usually are not more than 1–2 km wide and often even less than that. The percentage of area occupied by COar is negligible.

8) *Ridges of arachnoid annulus (Aar)*: These structures (Figure 2, Section 8) outline arachnoids (features which are akin to coronae but usually of smaller size;

Barsukov *et al.*, 1986; Nikishin *et al.*, 1992; Head *et al.*, 1992). Aar is related to wrinkle ridges of the plains even more closely than COar. Aar is practically a part of the wrinkle ridge network which locally in these areas have radial-concentric patterns thus outlining the arachnoids. These structures were observed only in seven of the 36 sites. They cover a negligible surface area.

9) *Smooth plains (Ps)*: – 10) *Lobate plains (Pl)*: These are plains-forming units not disrupted by wrinkle ridges. We designated the ridge-free plains *smooth plains* (Ps) if they are quite homogeneous in radar brightness and have no particular lobate or flow-like characteristics (Figure 2, Section 9). We called plains with lobate or flow-like characteristics *lobate plains*; such terrain (Figure 2, Section 10) often has high aspect ratios and has prominent lava flow morphology, particularly where it is located on the slopes of distinctive volcanic edifices such as Sif or Ozza Mons. For the more regional deposits this distinction depends on the scale and aspect ratio, and thus in these cases there may be some overlapping between Ps and Pl. Ps was observed in 15 of the 36 sites and Pl in 12. The averaged abundance of Ps/Pl is probably not more than 10% of the surface.

11) *Fractures of corona annulus (COaf)*: These structures (Figure 2, Section 11) outline annuli of some coronae. They are not densely spaced, so it can be seen what terrain they disrupt. We do not include in this designation fractures which belong to COdf. These structures were observed only in three of the 36 sites. In one case, they disrupted smooth plains and in two cases, plains with wrinkle ridges. The percentage of area occupied by COaf is negligible.

12) *Fractures (F)*: These structures (Figure 2, Section 12) are present practically everywhere. We mentioned them as a separate structure type in the stratigraphic sequences only if they were among the latest episodes of geologic activities at the sites.

13) *Rift-associated fractures (Fra)*: These structures (Figure 2, Section 13) form swarms and clusters of subparallel and anastomosing faults with feathering individual fractures. These swarms and clusters are as a rule found in association with topographic troughs (chasmata). In some places Fra are very densely spaced, thus, resembling the densely fractured terrain, especially Pdf, mentioned previously. But typically, the width of Fra changes from fracture to fracture, a characteristic that is unusual for Pdf. Besides, Fra are usually more prominent and look sharper on the images than Pdf/COdf. Volcanism is commonly observed in association with Fra both in the form of flows of different size emanating from the rift zones, and associated large shield volcanoes (Roberts *et al.*, 1992; Senske *et al.*, 1992; Head *et al.*, 1992). Fra were observed in 10 of the 36 sites. The average area covered by zones with abundant Fra is probably not more than 5% of the surface.

14) *Craters with associated dark paraboloids (CdP)*: In the identification of these features (Figure 2, Section 14) we followed the list of Campbell *et al.*, (1992). The first 36 craters of this list have an associated paraboloid of the so-called "pd" type (filled in parabola) and determine the sample sites of our study (Table 1; Figure 1). The areal percentage covered by the craters themselves is

negligible while the associated paraboloids occupy about half of the area of each of the sampled sites. The total area occupied by the pd type dark paraboloids mapped by Campbell *et al.* (1992) is about 5.8% of the surface of Venus, and the total area occupied by all varieties of dark paraboloids is about 8.1% of the surface. In each of the sites under study there are impact craters without associated dark paraboloids. Their stratigraphic significance requires a special study and in this paper we simply indicate that they are older than Cdp.

15) *Surficial streaks (Ss)*: These are roughly parallel, generally E–W trending streaks of tens to a few hundred km length, and usually superposed as a surficial mantle on underlying terrain (Figure 2, Section 15). Commonly they are darker than the background terrain, and they have been interpreted to be of eolian origin (Greeley *et al.*, 1992). They are not seen on the dark background of prominent dark paraboloids and are observed either in the brighter spots within the paraboloid or at its distal end. Ss are observed in 18 of the 36 sites. Their average areal percentage within the sites is no more than a few percent.

16) *Surficial patches (Sp)*: These are radar-dark patches of various form and size in local topographic lows and against or behind positive topographic obstacles (Figure 2, Section 16); they appear superposed on underlying terrain as a surficial mantle and are interpreted as eolian in origin. They are observed in nine of the 36 sites and three of those sites also have wind streaks. Sp areal percentage is negligible. The presence of eolian surficial streaks (Ss) and surficial patches (Sp) on top of the stratigraphic column does not mean that this kind of geologic activity occurred only in recent time; at least some of these features are very young while others may be older.

3. Stratigraphic Relations Among the Units and Structures

Our approach was to use standard techniques for the determination of relative stratigraphic position (see Wilhelms, 1990) for each of the 36 areas, establishing a stratigraphic column and geologic sequence of units and structures at each site, and then to examine the relationships (correlation) between the columns to search for common themes in the sequence of events. For example (Figure 3b), for an individual site, cross-cutting of fractures on another plains unit established the latter as older, while the embayment of these two units by a plains unit established the younger age of the plains, and superposition of a dark paraboloid crater on all units designates this as the relatively youngest event. These relationships then established the relative sequence of events: initial plains formation, followed by fracturing, followed by emplacement of younger plains, followed by impact and formation of the dark paraboloid crater (Figure 3b).

In our individual site stratigraphic analyses, we used plains with wrinkle ridges (Pwr) as something of a local reference terrain because of its widespread nature. First, all other units were analyzed to determine whether they predated, were syn-

chronous with, or postdated Pwr; as a rule, this could be determined reliably. Secondly, we attempted to determine for each of the sites the stratigraphic relationship between the several units and structures predating and postdating Pwr. The criteria for establishing stratigraphic relations were the same as cited above: 1) the presence or absence of embayment by plains-forming units and 2) the presence or absence of disruption and cross-cutting by ridges or fractures. In some sites some units were not in contact with each other in the region of study and thus we could not establish directly the stratigraphic relations between these units that were observed to be superposed in other areas. In these cases we noted the correlation with a query and placed them in the sequence most consistent with nearby stratigraphy.

The results of our analysis for 36 sites are presented in Table III in the form of stratigraphic columns and geologic sequences for each of the sites. We now examine the units, structures, and stratigraphic relationships in key areas within several of the sites to illustrate the techniques and to show how our general conclusions were reached. Reference to Table IV shows the units that appear in the areas highlighted, mapped, and discussed in the following Section. In most cases, units and structures are designated and mapped as shown in Figure 2, and the accompanying legend (Figure 3a) and captions. In some cases, however, map unit patterns have been changed to ensure clarity of relationships or details within a unit, and these are noted in the captions of each figure. In several cases, particularly in the case of Ridge Belts, Rift-Associated Fractures, and annular fractures and ridges around coronae and arachnoids, rather than mapping each of the individual structures themselves we have drawn a line around the area of most distinctive development of the structure to show the general distribution and relation to mapped units. This is noted in the individual figure captions. In general, the maps accompanying this paper are sketch maps intended to illustrate the basic characteristics, distribution, and relationships between various units and structures.

The typical characteristics of tessera are well illustrated in the vicinity of the crater Ruth (Site #3: 43.30°N, 19.84°E; C1-MIDRP 45N011;1 and F-MIDRP 45004;1) (Figure 4). Here, the near-orthogonal structural fabric of tessera terrain (Tt) is preserved as a remnant along the western margin of the mapped area, extending to the northeast as fragments of tessera surrounded and embayed by densely fractured plains (Pdf). Tt and Pdf in turn are embayed by plains with wrinkle ridges (Pwr) over a large portion of the area; a few fragments of Pdf in the SE attest to its once more-widespread nature. Numerous small domes are seen in Pwr. Several units of smooth plains (Ps) are observed in tne northern part of the area; these embay Pwr.

Additional examples of tessera are shown in the vicinity of the crater Magnani (Site #33: 58.63°N, 337.19°E; Cl-MIDRP 60N347;2 and F-MIDRP 55N337;201) (Figure 5). About 200-300 km S and SW of Magnani, one observes portions of Clotho tessera (Tt), which have been embayed by plains which were subsequently highly fractured (Pdf); some of the fractures clearly extend into the tessera, particularly in the central part of the map area. Volcanism continued in this region with

Table III*. Geologic columns (sequence of units and structures) for each of the 36 sites (See Table I) analyzed in this study

1 Annia Faustina	2 Holiday	3 Ruth	4 Stuart	5 Noreen	6 Bathsheba	7 Francesca	8 Bassi	9 Jadwiga	10 Li-Quing- Zhao	11 Boulanger	12 Caldwell	13 Yonge	14 Merit-Ptah	15 Pimiko	16 Phyllis	17 Greenaway	18 Ban- Zhao
			Ss	Ss			Ss/Sp			Ss			Ss		Sp	Ss/Sp	Sp
Cdp	Cdp	Cdp	Cdp	Cdp	Cdp	Cdp	Cdp	Cdp	Cdp	Cdp	Cdp	Cdp	Cdp	Cdp	Cdp	Cdp	Cdp
Pl	F											Fra					
Fra	COaf		Ps									Ps					
Pl	Ps	F	F	F/Pl	F/Pl	F	F	F	F	F	F	Fra	Ps/F	F	F	F	F
Pwr	Pwr	Pwr	Pwr	Pwr	Pwr	Pwr	Pwr	Pwr	Pwr	Pwr	Pwr	Pwr	Pwr	Pwr	Pwr	Pwr	Pwr
	RB															Pfr	
Pdf/COdf	Pdf/COdf	Pdf	Pdf	Pdf/COdf	Pdf/COdf	Pdf/COdf	Pdf/COdf	Pdf	Pdf/COdf	Pdf/COdf	Pdf		Pdf/COdf	Pdf/COdf	Pdf/COdf	Pdf	Pdf
Tt	Tt	Tt	Tt	Tt	Tt	Tt	Tt	Tt	Tt	Tt	Tt	Tt	Tt	Tt	Tt		

*COar and Aer units are not shown in this table. They are considered to be contemporaneous with wrinkle ridges Pwr (see text).

Table III. Continued

19 Austen	20 Martinez	21 Akiko	22 Yablochkina	23 Uvaysi	24 Edinger	25 Boleyn	26 Akeley	27 Glaspell	28 Lyon	29 Montessori	30 Cotton	31 Dashkova	32 Aurelia	33 Magnani	34 Comnena	35 Carson	36 Audrey
Sp	Ss/Sp	Ss	Ss		Ss		Ss	Ss/Sp	Sp	Ss		Ss/Sp	Ss		Ss	Ss	
				Pl													
	Fra			Fra		Fra	Pl										Pl(?)Fra(?)
Cdp	Cdp	Cdp	Cdp	Cdp	Cdp	Cdp	Cdp	Cdp	Cdp	Cdp	Cdp	Cdp	Cdp	Cdp	Cdp	Cdp	Cdp
Fra							Fra										
Ps	Fra	Fra	F	Pl		Fra/Ps	Ps			F	F	Fra	F		Ps	F	Fra
Coaf	Ps/F	Pl	Pl	Fra	Ps	Ps	COaf/Coar	Ps	Ps	Ps	F/Pl	Ps/Pl/F	Pl	Ps	F	Pl	Pl
Pwr	Pwr	Pwr	Pwr	Pwr	Pwr	Pwr	Pwr	Pwr	Pwr	Pwr	Pwr	Pwr	Pwr	Pwr	Pwr	Pwr	Pwr
		Pfr	Pfr	Pfr	RB										Pfr	Pfr	
COdf	COdf	Pdf	Pdf	Pdf	Pdf	Pdf/COd	Pdf	Pdf	Pdf	Pdf/COdf	Pdf/COdf	Pdf/COdf	Pdf/COdf	Pdf	Pdf/COdf	Pdf	Pdf/COdf
	Tt	Tt	Tt							Tt	Tt	Tt		Tt			

Table IV. Cross-correlation of defined units and analyzed areas discussed in detail and shown in Figures 4–15 in this paper

			Fig. 4: Site 3	Fig. 5: Site 33	Fig. 6: Site 18	Fig. 7: Site 24	Fig. 8: Site 20	Fig. 9: Site 29	Fig. 10: Site 26	Fig. 11: Site 22	Fig. 12: Site 2	Fig. 13: Site 1	Fig. 14: Site 13	Fig. 15 Site 20
16	Sp	Surficial patches				×								
15	Ss	Surficial streaks				×								
14	Cdp	Craters with dark parabolas			×		×					×	×	×
13	Fra	Rift-associated fractures					×					×	×	×
12	F	Fractures								×	×			
11	COaf	Fractures of corona annulus						×	×					
10	Pl	Plains, lobate					×		×		×	×		
9	Ps	Plains, smooth	×		×		×	×	×		×		×	×
8	Aar	Ridges of arachnoid annulus								×				
7	COar	Ridges of corona annulus					×	×						
6	Pwr	Plains with wrinkle ridges	×	×	×	×	×	×	×	×	×	×		
5	RB	Ridge Belts				×					×			
4	Pfr	Plains, fractured & ridged								×				
3	Pdf	Plains, densely fractured	×	×	×	×			×		×	×		
2	COdf	Corona, densely fractured			×		×	×						
1	Tt	Tessera	×	×									×	

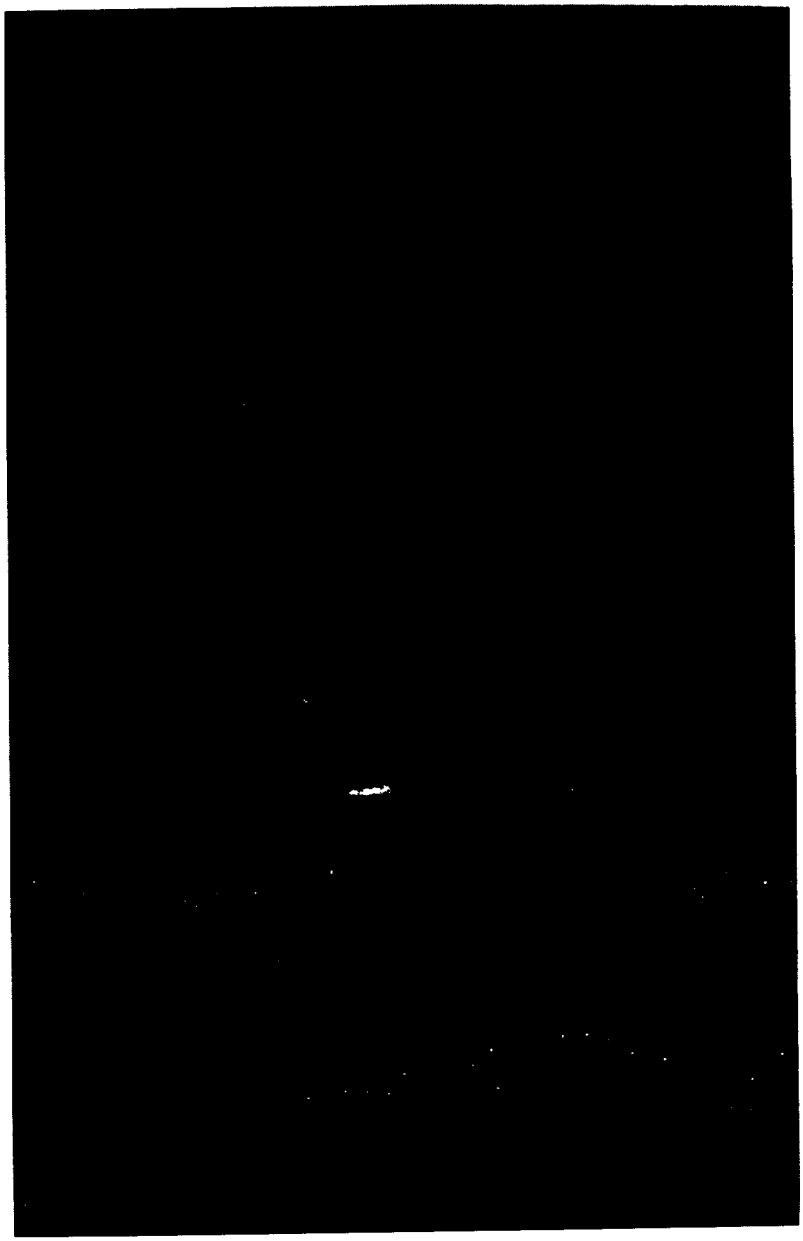

Fig. 4a.

Fig. 4. Magellan image (a) and geologic sketch map (b) of a portion of Site #3, the crater Ruth (43.30 °N, 19.84 °E) region. Portion of F-MIDR 45N004; 1. Refer to Figure 3a for legend. Circles and dots represent small volcanic shields.

patches of plains with wrinkle ridges and smooth plains superposed on both Tt and Pdf. The smooth plains are not modified by wrinkle ridges apparently because they postdate the formation of the ridges. Some areas of the tessera are relatively smoother than others, suggesting partial volcanic resurfacing; these relatively smoother areas are transitional to Pdf.

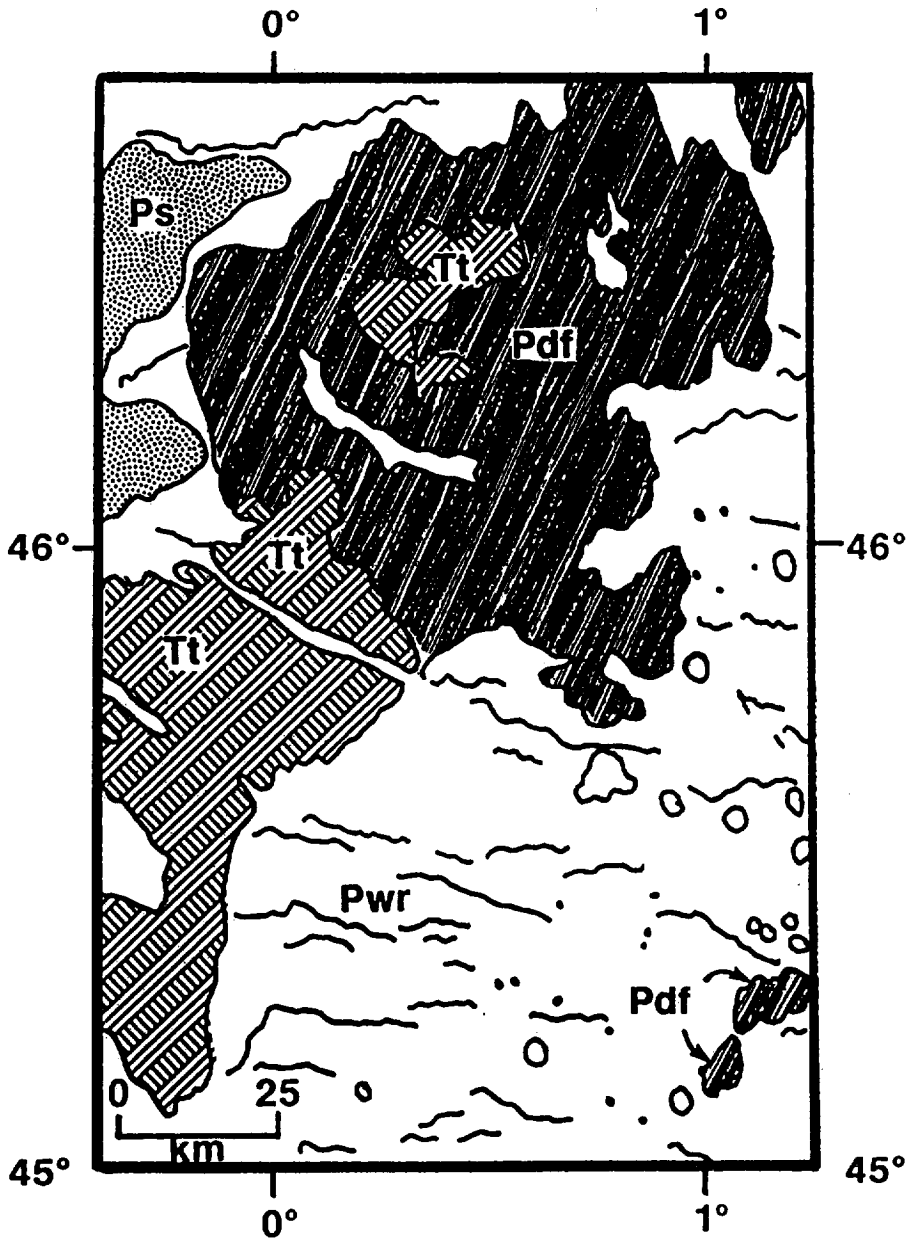

Fig. 4b.

In the vicinity of the 36 km diameter dark paraboloid crater Ban-Zhao (Site #18; 17.17°N, 146.96°E; C1-MIDR 15N146), a distinctive series of stratigraphic relationships can be seen (Figure 6). The oldest unit in the region illustrated is densely fractured terrain (unit Pdf), which is exposed in a NW-trending belt which begins in a remnant circular to oval structure (A in Figure 6) and extends at least a thousand km to the NW. Along this zone, which is typically 50–150 km wide, a dense series of fractures and narrow graben characterize the belt and are oriented parallel and subparallel to it. Along the belt are hints of highly degraded or aborted coronae (A, B) (unit COdf?), and in the intervening areas the dense fractures appear to be on relatively smooth terrain and thus to be unit Pdf. This terrain is then embayed by plains of intermediate brightness, the most extensive unit in the region.

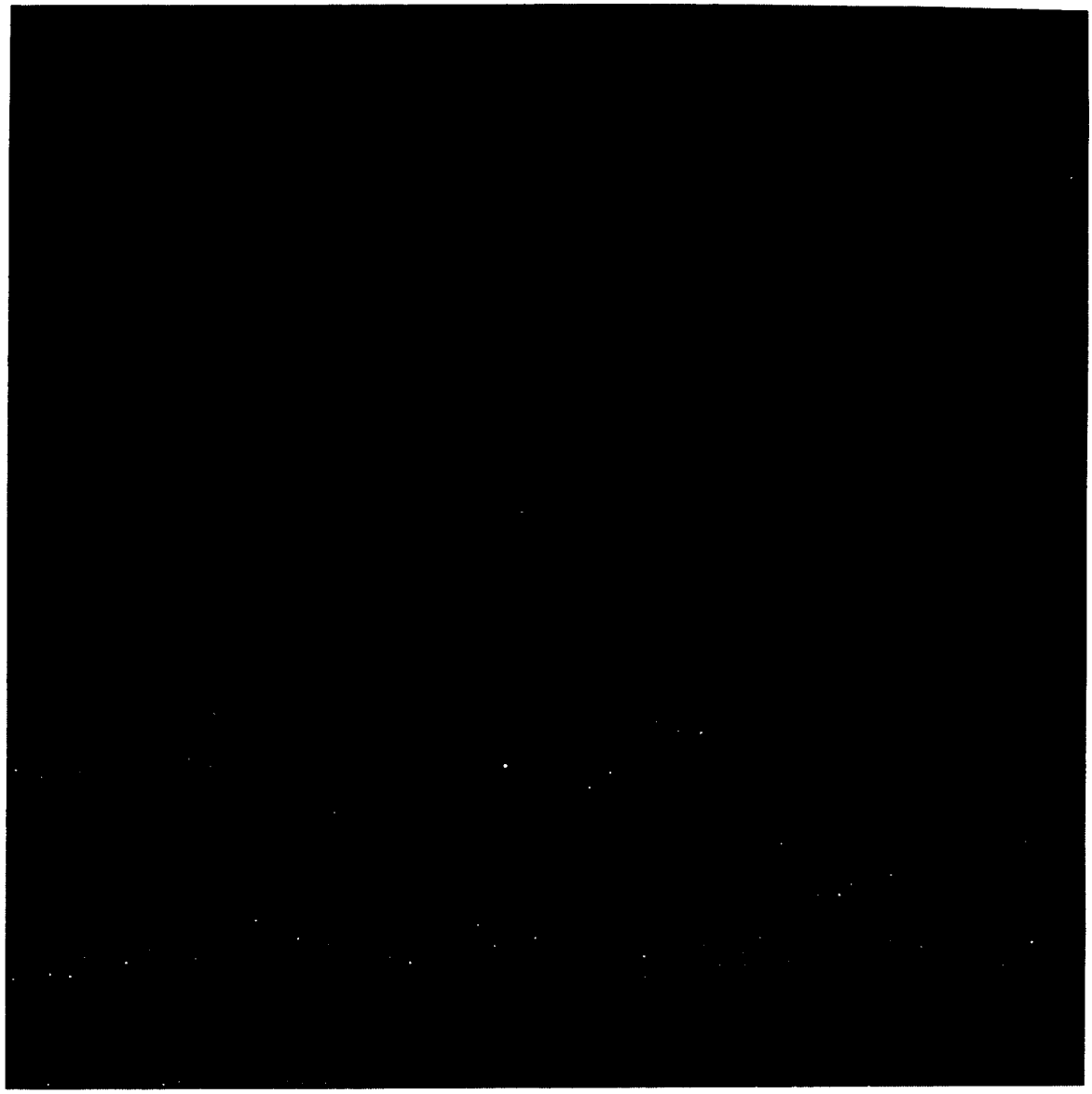

Fig. 5a.

Fig. 5. Magellan image (a) and geologic sketch map (b) of a portion of Site #33, the crater Magnani (58.63°N, 337.19°E) region. F-MIDR 55N337;201. Refer to Figure 3a for legend. The map pattern for Pdf shown in Figure 3a is omitted in this example in order to show the location of Ps and Pwr more clearly.

Cutting these plains is a sinuous channel (C) extending from the NE to the SW across the region, and showing greater sinuosity where it winds its way through the belt of densely fractured terrain. Several other segments of sinuous channels can be seen in the plains. Extensive *en echelon* wrinkle ridges cut the lava plains and trend in a generally ENE direction, and the terrain is now classified as unit Pwr. Although the wrinkle ridges cut and clearly postdate the plains and the lava channels, they do not obviously cut the densely fractured terrain. Subsequent to these events, radar bright lava flows emanating from a large corona about 600 km NE of Ban-Zhao entered the area in the NE (D), covering the plains of intermediate radar brightness,

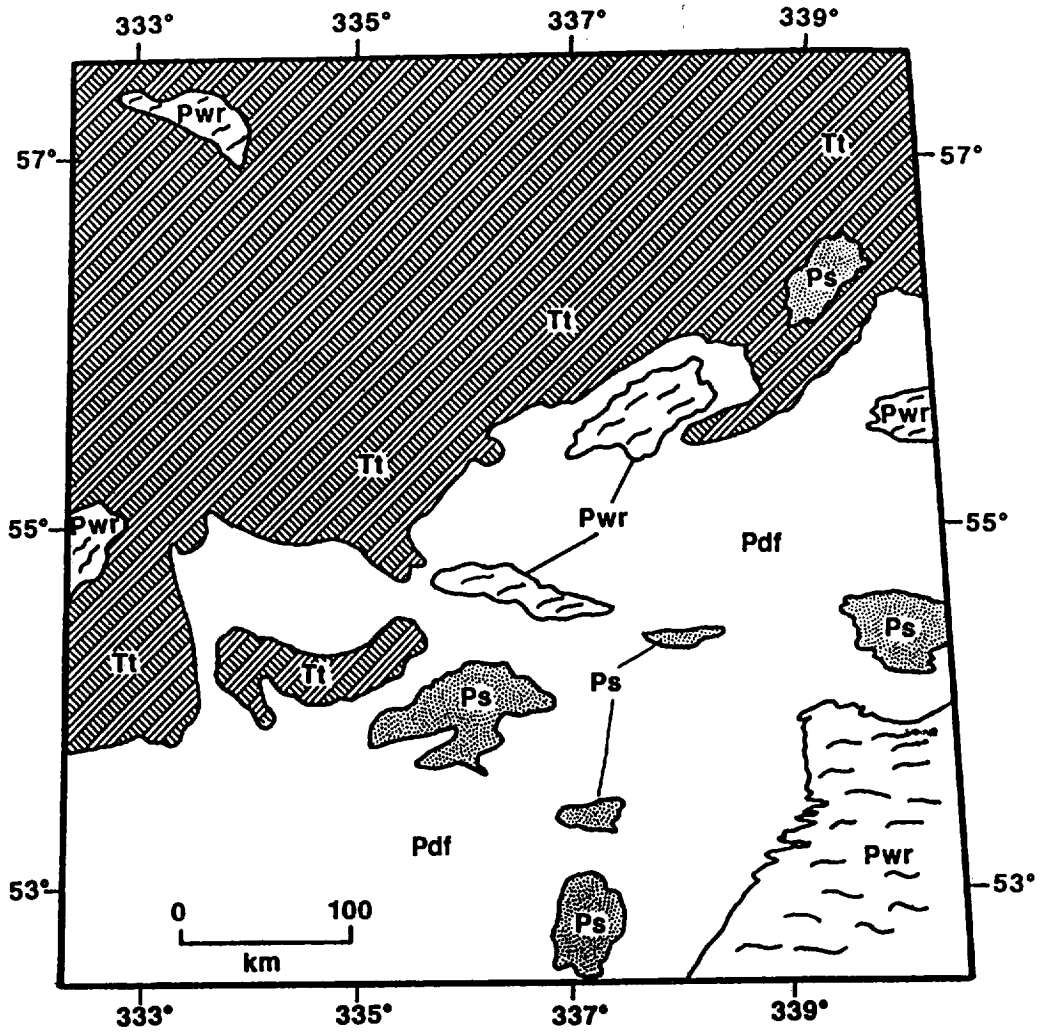

Fig. 5b.

and even extending 10-15 km up an old lava channel in the underlying unit (E). Wrinkle ridges existed on the intermediate plains at the time of this event because the flow margin is controlled in part by their presence (F). However, wrinkle ridges within the radar bright plains also appear to have formed subsequently, testimony to the fact that the ridge producing deformation extended over some time period. Following these events, an impact crater formed approximately at the boundary of the two plains units (between E and F), and this was followed by the formation of Ban-Zhao and its extensive dark parabola, which post-dates all events in this region.

About 1800 km SE of the dark-paraboloid crater Edinger (Site #24; 68.80°S, 208.42°E); C1-MIDR 75S248) (Figure 7) a somewhat similar sequence of units is observed. The oldest unit consists of a few patches of densely fractured terrain (Pdf) (Figure 7), each with a similar orientation of fractures and graben (~N–S). These Pdf occurrences are embayed by regional plains and a sinuous lava channel is incised into the plains and extends across the area (C). The plains must have been relatively flat at the time of emplacement of the channel. Subsequent to this

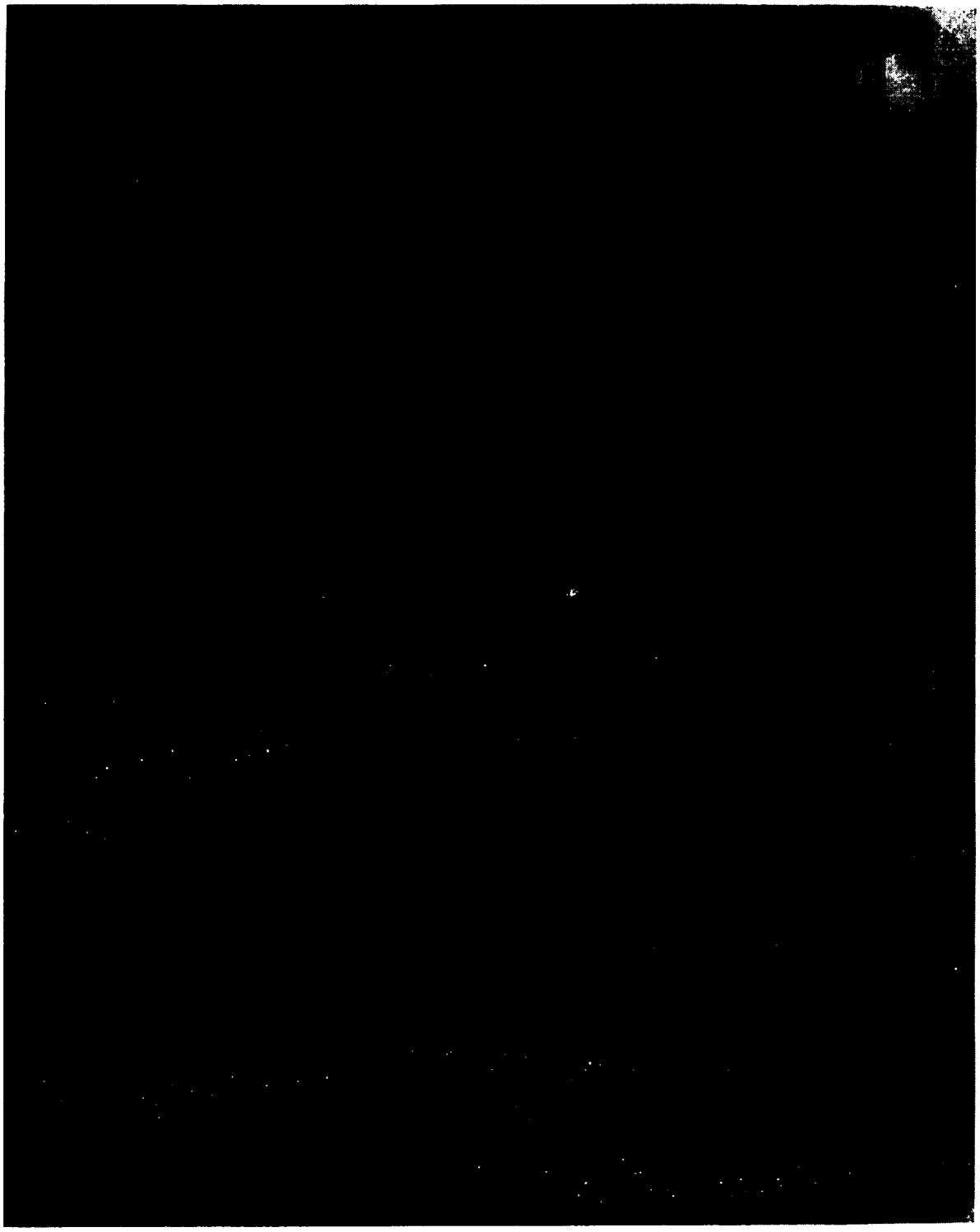

Fig. 6a.

Fig. 6. Magellan image (a) and geologic sketch map (b) of a portion of Site #18, the crater Ban-Zhao (17.17°N, 146.96°E) region. Portion of C1-MIDR 15N146;1. Refer to Figure 3a for legend. Circles and dots represent small volcanic shields. Circled letters refer to items discussed in the text. C indicates channels.

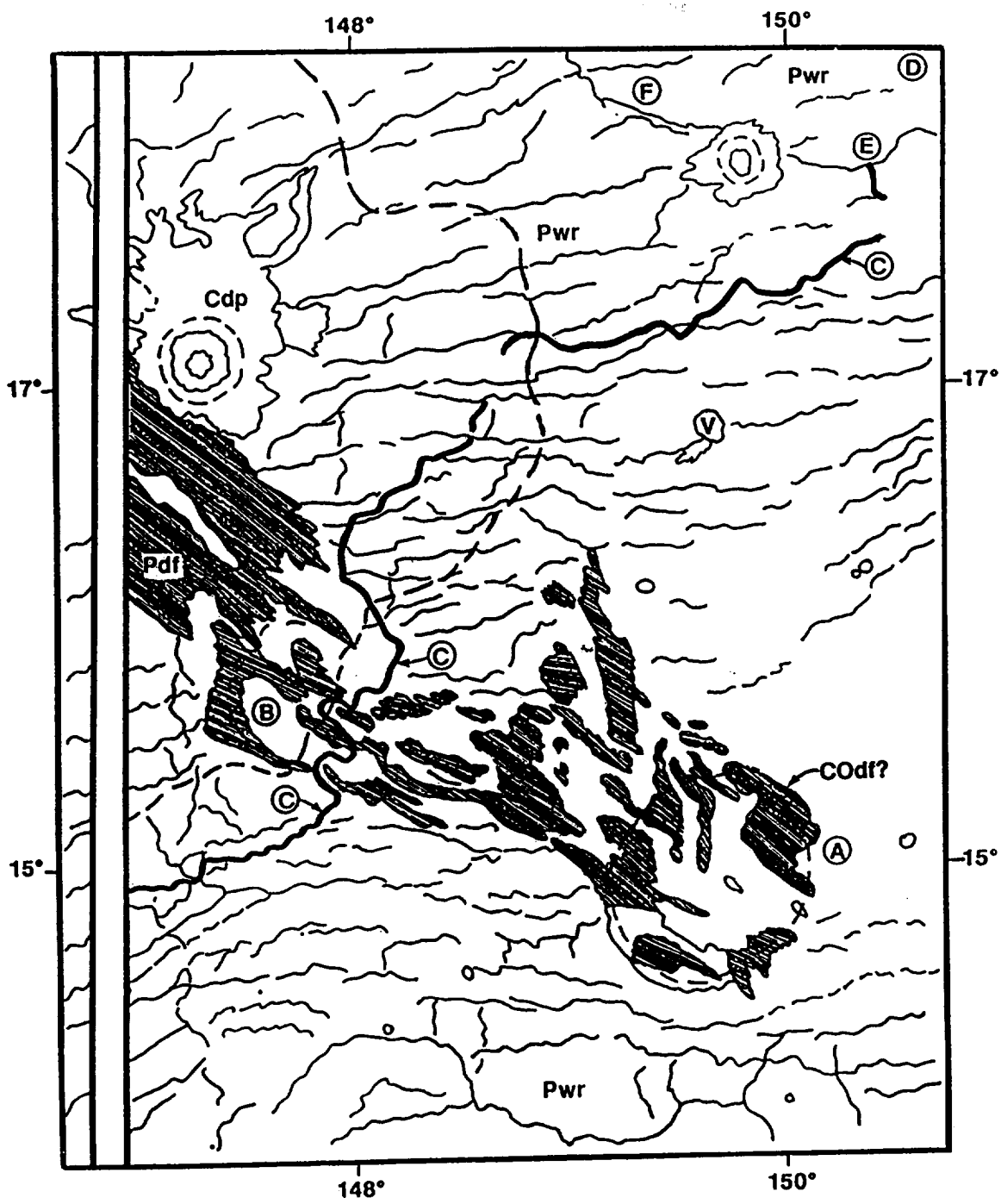

Fig. 6b.

the plains were deformed into ridge belts (RB), and wrinkle ridges formed on the plains. The Pdf occurrences are located within the central parts of the ridge belts, suggesting that they may have served as loci for the release of horizontal compressional strain during ridge belt formation. Some evidence suggests that the ridge belts predate the ridges in the plains; some wrinkle ridges terminate against or die out as they enter into the ridge belts, and in the NW ridge belt, there is a much higher abundance of smaller wrinkle ridges than in the surrounding ridged plains.

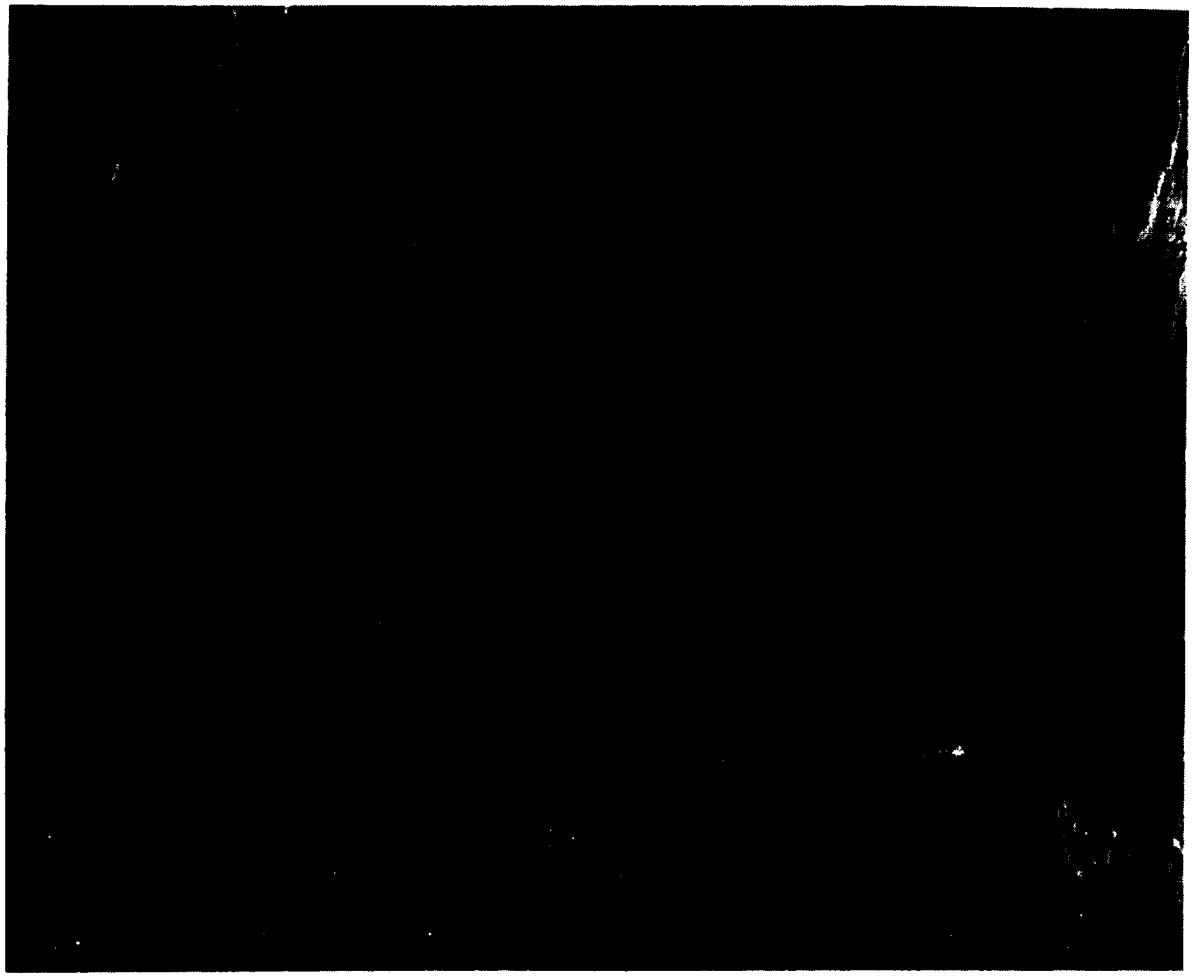

Fig. 7a.

Fig. 7. Magellan image (a) and geologic sketch map (b) of a portion of Site #24, the crater Edinger (68.80°S, 208.42°E) region. Portion of C1-MIDR 75S248;201, about 1800 km SE of Edinger. Refer to Figure 3a for legend. The ridge belt structures are outlined by a solid line and designated RB. C indicates channel.

Following the deformation producing the ridge plains (Pwr), eolian modification spread material as streaks (Ss) and patches (Sp), particularly in the vicinity of the EW trending ridge belt. Just north of this ridge belt the patches of eolian debris are spread northward as lobate radar dark extensions in the lows between the NS trending wrinkle ridges. In addition, EW trending radar-dark streaks are observed along the ridge belt crest.

Corona relationships are well-illustrated in the vicinity of Site #20 (Craters Martinez, 11.64°S, 174.75°E, and Warren 11.80°S, 176.50°E, C1-MIDR15S163;1, C1-MIDR15S180;1) (Figure 8). Sith, a 360 km × 450 km asymmetric corona (Stofan *et al.*, 1992) lies east of an unnamed corona about 300 km in diameter; both are along the strike of Dali Chasma, fractures of which extend through the area. Well illustrated at both coronae are dense fractures associated with the coronae (COdf) and generally oriented radially from the coronae interior. Also seen are concentric fractures around portions of Sith and along the NE portion of Sith, a major zone

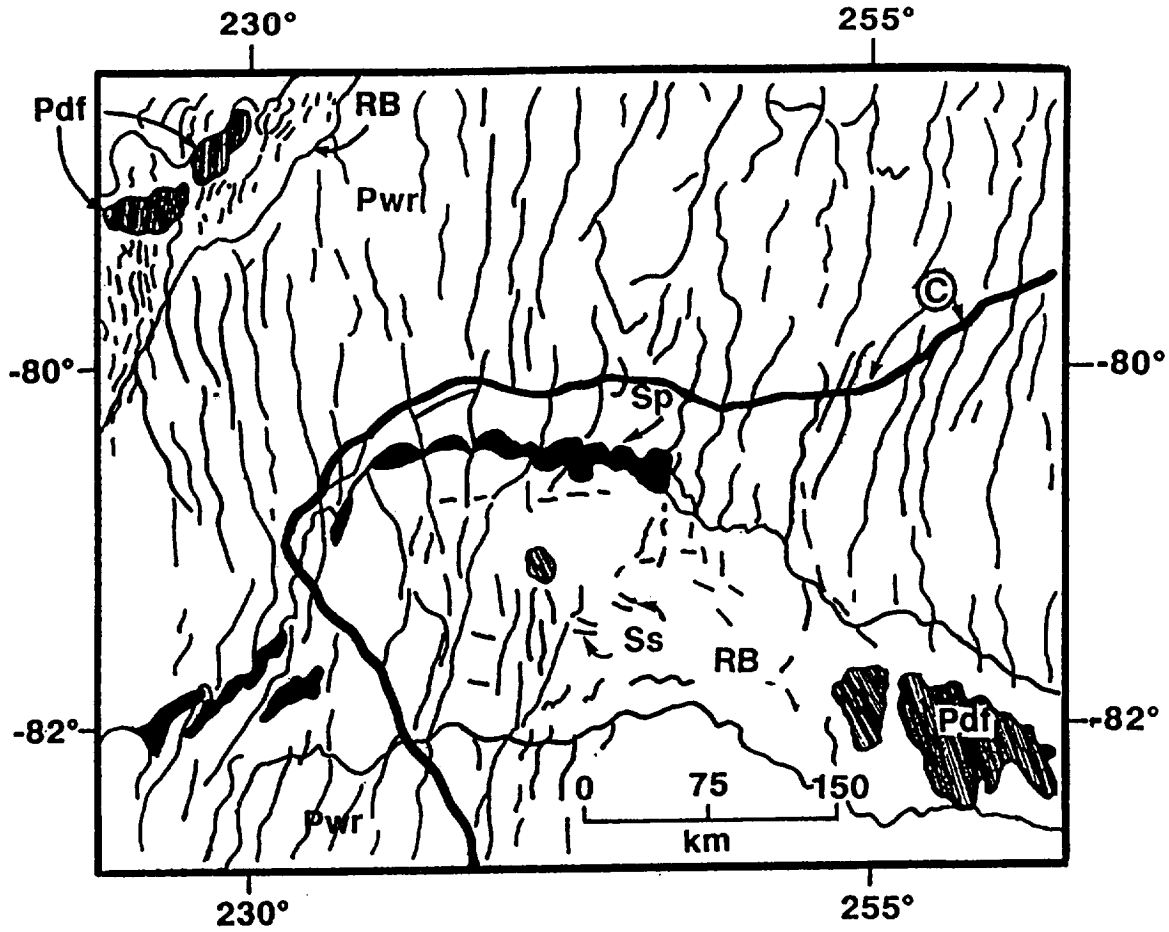

Fig. 7b.

of concentric or annular ridges (COar). This zone of annular ridges extends to the NW and is continuous with elements of wrinkle ridges that form ridged plains (Pwr). North of the unnamed corona, a series of lobate flows (Pl) extending from the edge of the concentric and radial fractures, forms a unit that embays the ridged plains. Other patches of smooth plains (Ps) are distributed throughout the coronae and adjacent areas. All these units are cut by fractures associated with Dali Chasma (Fra). The two craters, Martinez and Warren, are both superposed on virtually all of these units, but the floor of Martinez is flooded with dark material (Ps) and in turn is cut by rift-associated fractures (Fra) (see also Figure 15), indicating that rifting and flooding are contemporaneous and that both continued beyond the time of the impact of Martinez.

Additional corona relationships are shown in the vicinity of Site #29, the crater Montessori (59.43°N, 279.92°E, C1-MIDR 60N291;1) (Figure 9). About 1,000 km SE of Montessori occurs the ovoidal 670 km × 330 km Demeter corona (55.0°N, 295.0°E). The northern, southern, and part of the eastern rims of Demeter are outlined by arcuate annular swarms of ridges (COar). These annular ridges are a continuation of regional patterns of wrinkle ridges that form on plains (Pwr) both outside and within Demeter. Within Demeter can be seen remnants of densely

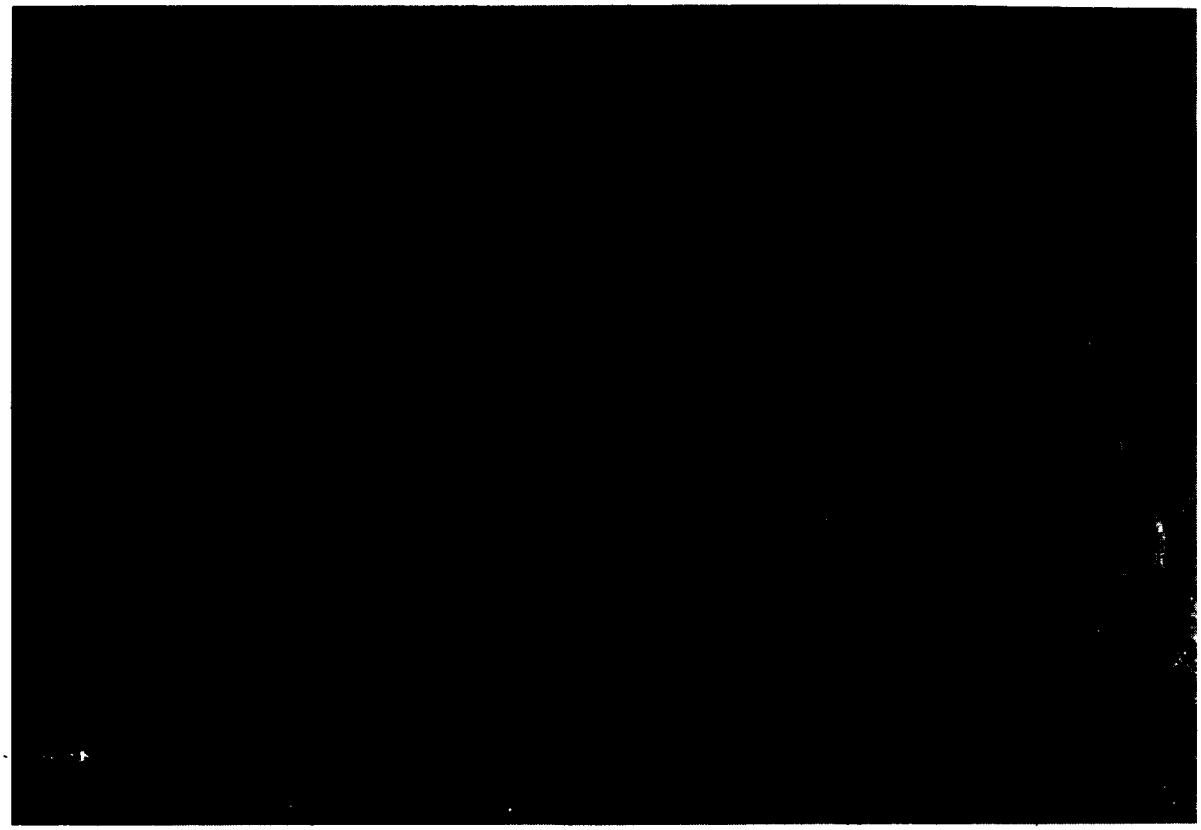

Fig. 8a.

Fig. 8. Magellan image (a) and geologic sketch map (b) of a portion of Site #20, the craters Martinez (11.64°S, 174.75°E; 24 km in diameter) and Warren, (11.80°S, 176.50°E) region. Craters are shown by outline of ejecta and central structure. Corona relationships are well-illustrated in the vicinity of these craters by Sith, a 360 km × 450 km asymmetric corona (Stofan *et al.*, 1992) and an unnamed corona about 300 km in diameter lying to the west. Portion of C1-15S180;201, C1-15S163;1. Refer to Figure 3a for legend. A solid line encloses the area of well-developed annular ridge structures NE of Sith. Individual wrinkle ridges in unit Pwr are not shown.

fractured terrain much of which appears to be related to the earlier stages of development of the coronae (COdf) but some of which is very densely fractured and may be Pdf. Wider expanses of Pdf are seen to the north of Demeter. Along the eastern edge of Demeter occurs a band of fractured terrain (COaf) that is part of the rim of the corona. These fractures cut the wrinkle ridges and are embayed by younger smooth plains (Ps) that occur within the corona. In summary, the stratigraphic relationships suggest the following sequence: extensive fracturing of preexisting terrain (Pdf) followed by the emplacement of additional regional plains, and the formation of wrinkle ridges outlining the northern and southern edges of Demeter (COar; Pwr). This was followed by the formation of the northern, southern, and eastern annulus fractures (COaf), and the embayment of these units by smooth plains.

Another example of a corona and its relationships to plains can be seen in the vicinity of Site #26, the crater Akeley (8.01°N, 244.53°E, C1-MIDR 15N249; 1) (Figure 10). The corona in the central part of the map region has an outer 150 km

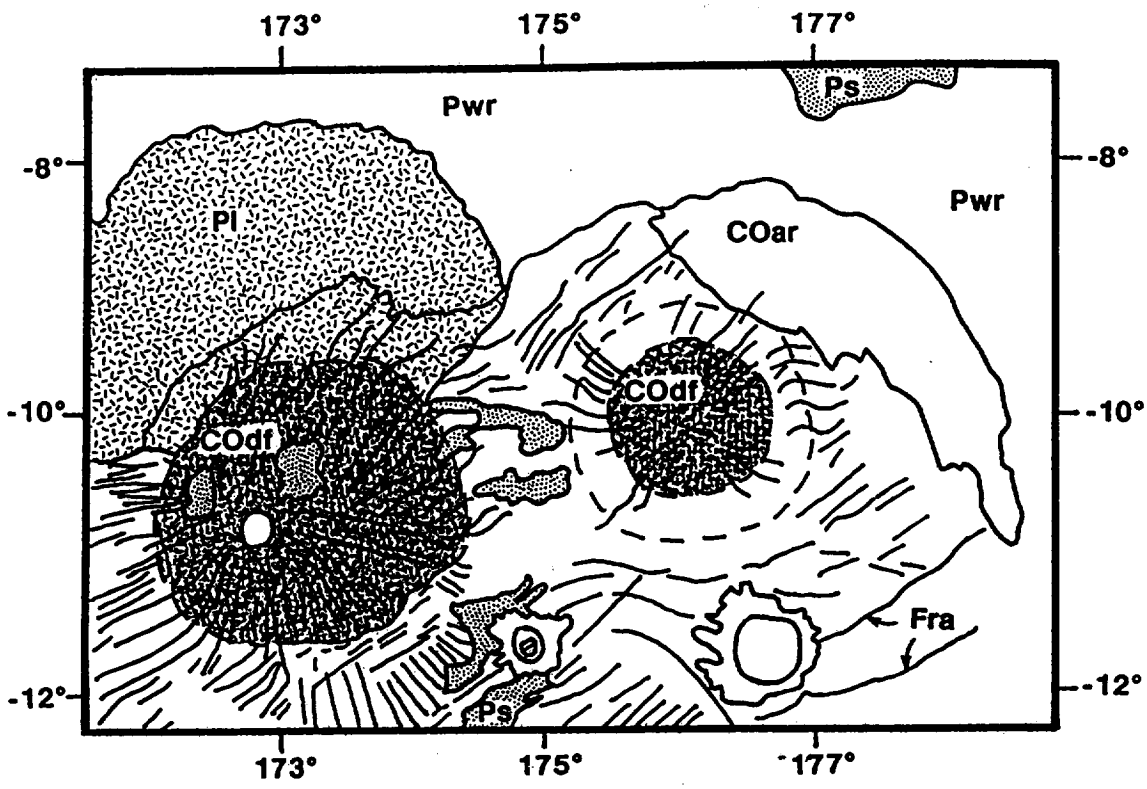

Fig. 8b.

ring and an inner 75 km ring, both outlined mostly by fractures (COaf). The earliest unit occurs as small patches of densely fractured plains (Pdf) spread throughout the mapped area. Following this, a wide variety of plains was emplaced which subsequently were deformed by wrinkle ridges (Pwr), now preserved in a broad belt extending SW to NE across the mapped region. Subsequently, smooth plains were emplaced in the NW, and fractures were formed, some concentrated in the area of the coronae and radial to it, and others cross-cutting in a general NW–SE trend. Portions (subunits) of the smooth plains also appear to truncate and embay some of the fractures (see A in Figure 10b). In addition, a major source region for lobate plains (Pl) is located in the SE part of the map area. Here, lava flows extend some 75–100 km from a central edifice about 25 km in diameter with an 8 km summit caldera, covering all preexisting units, including most fractures, and being cut by a few fractures.

Arachnoid relationships are illustrated in the vicinity of Site #22, the crater Yablochkina (48.28°N, 195.30°E, C1-MIDR 45N202;1) (Figure 11). About 800 km south of Yablochkina two belts of fractured and ridge plains (Pfr) converge in the vicinity of an arachnoid, which has a small annulus of ridges surrounding it (Aar). Plains with wrinkle ridges embay the belts of Pfr. Fractures (F) radial to the arachnoid both cut all preexisting units and are sometimes embayed by the ridged plains (Pwr). Digitate and lobate flow units are visible to the west of the arachnoid in the ridged plains, and it is obvious from the flow morphology that some flows

Fig. 9a.

Fig. 9. Magellan image (a) and geologic sketch map (b) of a portion of Site #29, the crater Montessori (59.43°N, 279.92°E, C1-MIDR 60N291;1). About 1,000 km SE of Montessori occurs the ovoidal 670 km × 330 km Demeter corona (55.0°N, 295.0°E), mapped here. Refer to Figure 3a for legend. The major annular ridge structures (COar) are mapped and outlined by lines indicating the extent of the distribution of this structure. The annular fractures (COaf) are too dense to map individually, so their location is outlined by lines showing the extent of the distribution of this structure.

were emplaced before the formation of some ridges and some during (they follow ridge topography but are cut by ridges in turn).

Ridge belts and their relationships to surrounding units are well-illustrated in the vicinity of Site #2, the crater Holiday (46.73°S, 12.83°E, C1-45SO11;1) (Figure 12). Here, patches of densely fractured plains (Pdf) are spread throughout the region and a ridge belt (RB) averaging 50–75 km in width extends in an arc-like pattern across the center of the area, with a bifurcation near the center of the mapped region. An exposure of plains with wrinkle ridges (Pwr) is seen between the forked portion of the ridge belt, and these units in turn are flooded and embayed by widespread undeformed plains, with a mixture of smooth plains (Ps) and lobate plains (Pl). In the period of emplacement of smooth plains, linear fractures (F) oriented generally NNE were formed in preexisting units primarily in the SW portion of the area, and then were flooded and embayed by later units of Pl and Ps.

Rift-associated fractures and their relationships to surrounding units are seen in the Western Eistla region at Site #1, just SW of the crater Annia Faustina (22.09°N, 4.69°E; C2-MIDR 30N026; 1) (Figure 13). Densely fractured plains

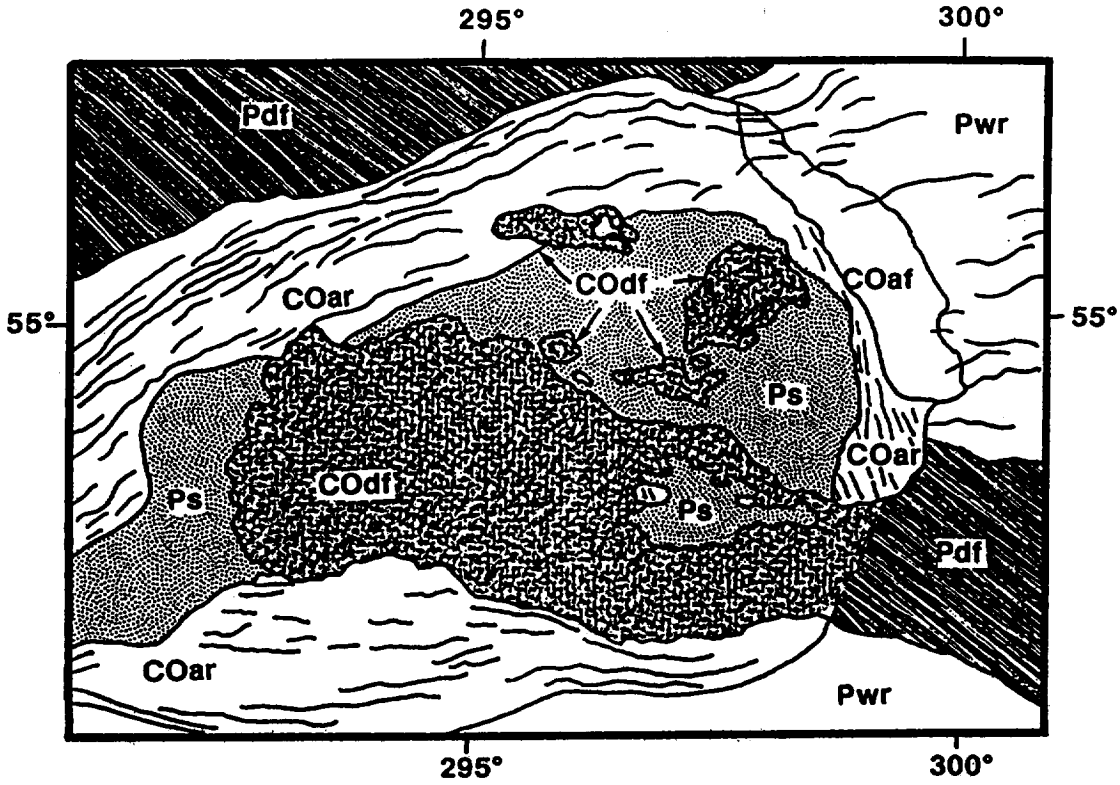

Fig. 9b.

(Pdf) are exposed in the central part of the map region, and are embayed by plains with wrinkle ridges (Pwr). These in turn are cut by rift-associated fractures (Fra) making up Guor Linea extending SE from Gula Mons. Lobate plains (Pl) derived primarily from Gula Mons flood the rift-associated fractures (Fra) and a few individual fractures appear to cut these plains. The final major event in the mapped area is the formation of the 22 km dark paraboloid crater Annia Faustina; its prominent dark paraboloid is seen to overlie all of the units in the NW part of the mapped area.

The interrelationship of a young crater and rift-associated fractures in plains is seen in the vicinity of the crater Yonge in Virava Chasma at Site #13 (13.96°S, 115.06°E) (Figure 14). In this area, smooth volcanic plains (Ps) have embayed tessera (Tt) and these plains in turn have been fractured by a series of WNW trending graben and fractures of Virava Chasma (Fra). Often, additional patches of plains have been emplaced and many of these in turn are cut by the rift-associated fractures, establishing the alternation and synchroneity of these two processes. The 28 km diameter dark-paraboloid crater (Cdp) Yonge is superposed on these units, as indicated by the burial of Fra and Ps by ejecta within about 5–10 km of the rim crest, and the control of ejecta emplacement by fractures and related topography at greater radial ranges. No fractures or Ps are observed on the crater floor or interior. The youngest unit is the dark paraboloid crater (Cdp) and its associated deposits. The dark paraboloid is seen as a darkening of some of the plains units and portions

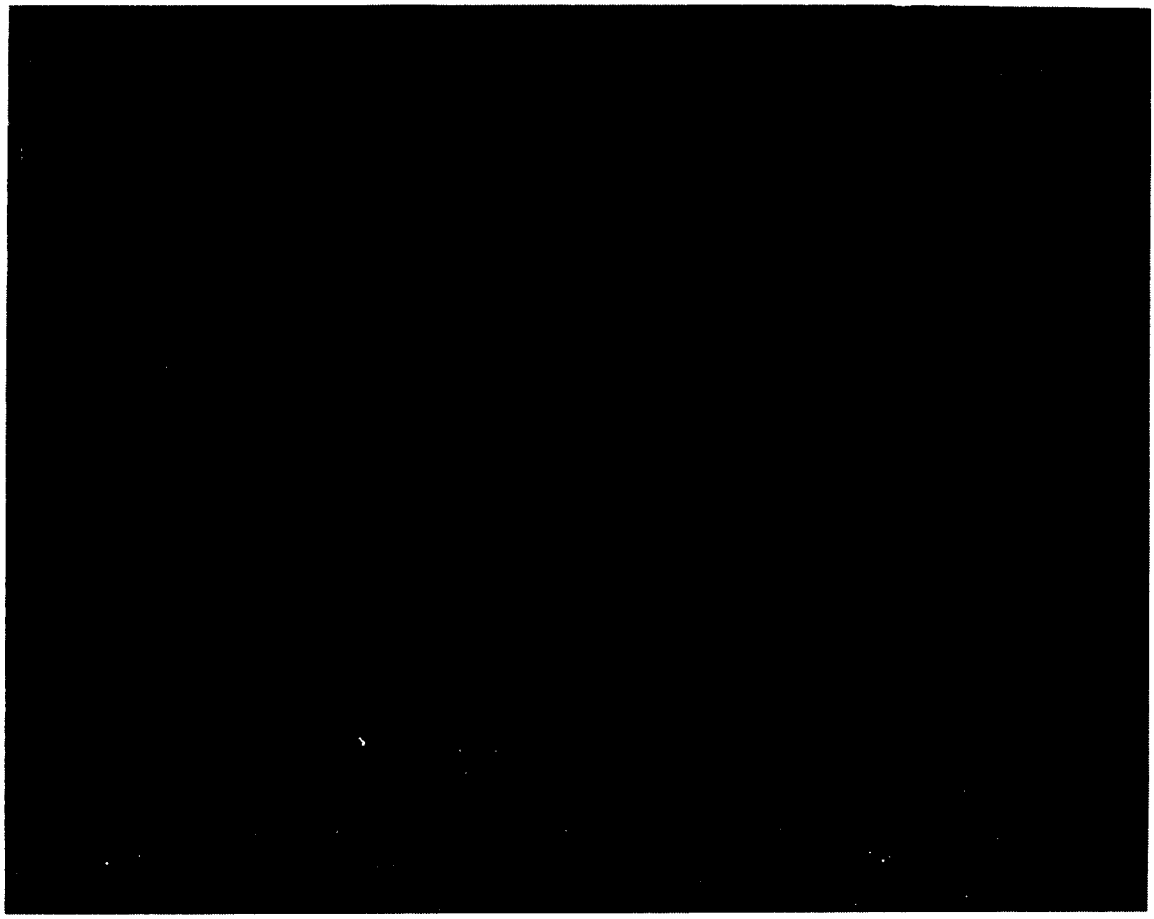

Fig. 10a.

Fig. 10. Magellan image (a) and geologic sketch map (b) of a portion of Site #26, the crater Akeley (8.01°N, 244.53°E, C1-MIDR15N249;1). Corona is at 9.5°N, 254.5°E. Refer to Figure 3a for legend. The annular fractures (COaf) are not mapped individually; their location is outlined by lines showing the extent of the distribution around the corona. In this map, individual ridges in unit Pwr are not mapped so that the fractures are more clearly visible.

of the tessera just to the NE of the crater. Yonge is the youngest event in the mapped area.

The importance of post-crater modification is seen in the case of Site #20 and the crater Martinez in Dali Chasma (11.64°S, 174.75°, C1-MIDR15S180;1, C1-MIDR15S163;1) (Figure 15). The regional setting of Martinez is shown in Figure 8. Here, regional fractures associated with Dali Chasma (Fra) strike ENE across the mapped area (Figure 8) cutting smooth plains and several other units associated with nearby coronae. The 24 km crater Martinez is superposed on these units, as indicated by burial of preexisting topography by the blanket of ejecta near the rim and by the control of the emplacement of ejecta by the presence of various topographic features (e.g., graben) related to underlying units. In this case, in contrast to the crater Yonge (Figure 14), the interior of the crater is modified by dark plains primarily in the SE quadrant, and these in turn are cut by a series of ENE trending fractures which appear identical to those indicated to be part of Fra

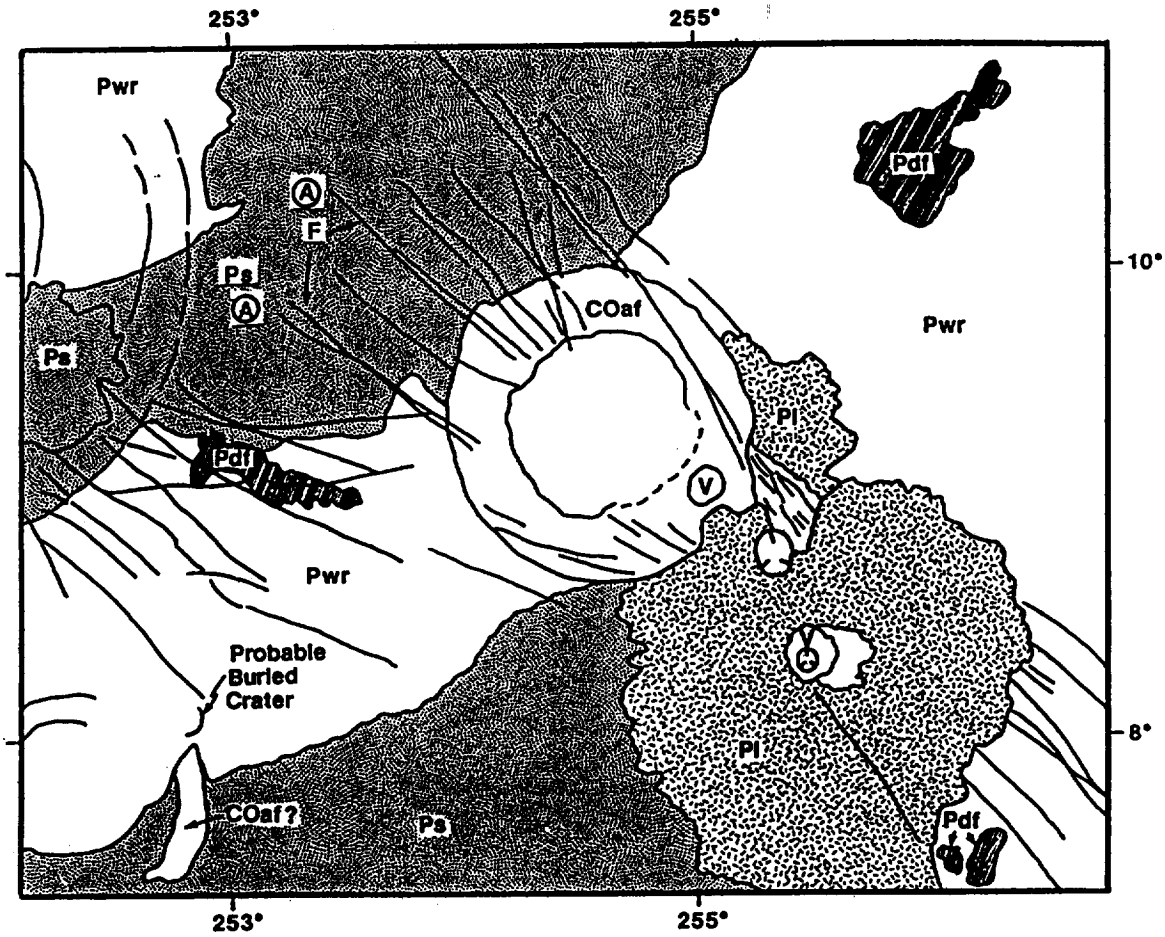

Fig. 10b.

formed prior to the Martinez event. Thus, emplacement of smooth plains (Ps) and rift-associated fracturing (Fra) clearly extend beyond the time of formation of the crater Martinez, mapped as a dark paraboloid crater by Campbell *et al.* (1992).

Although the dark smooth plains in the interior of Martinez appear identical to those in the exterior, it is possible that they may represent some aspect of crater formation, such as impact melt deposits (see Schaber *et al.*, 1992), rather than plains volcanism. Thus, the post-Martinez occurrence of volcanism in the mapped area should be viewed as tentative until better criteria can be established for distinguishing crater-related deposits and volcanic flooding. The post-Martinez formation of rift-associated fractures (Fra) remains clear; however, the distribution of these fractures within the crater offers guidance in the interpretation of these features in other craters. Note that the fractures cutting the dark plains on the crater floor (Figure 15) do not appear to extend up either the eastern or western wall or onto the rim. Although there are some parallel fractures on the rim crest and wall at about 1–2 and 6–7 o'clock, these are not as clearly identified as those on the floor, and most of the areas of crater wall and floor do not show any indication of the extension into the adjacent wall. It is presumed that the stress field operating to produce the floor fractures was also sufficient to produce fractures in the adjacent

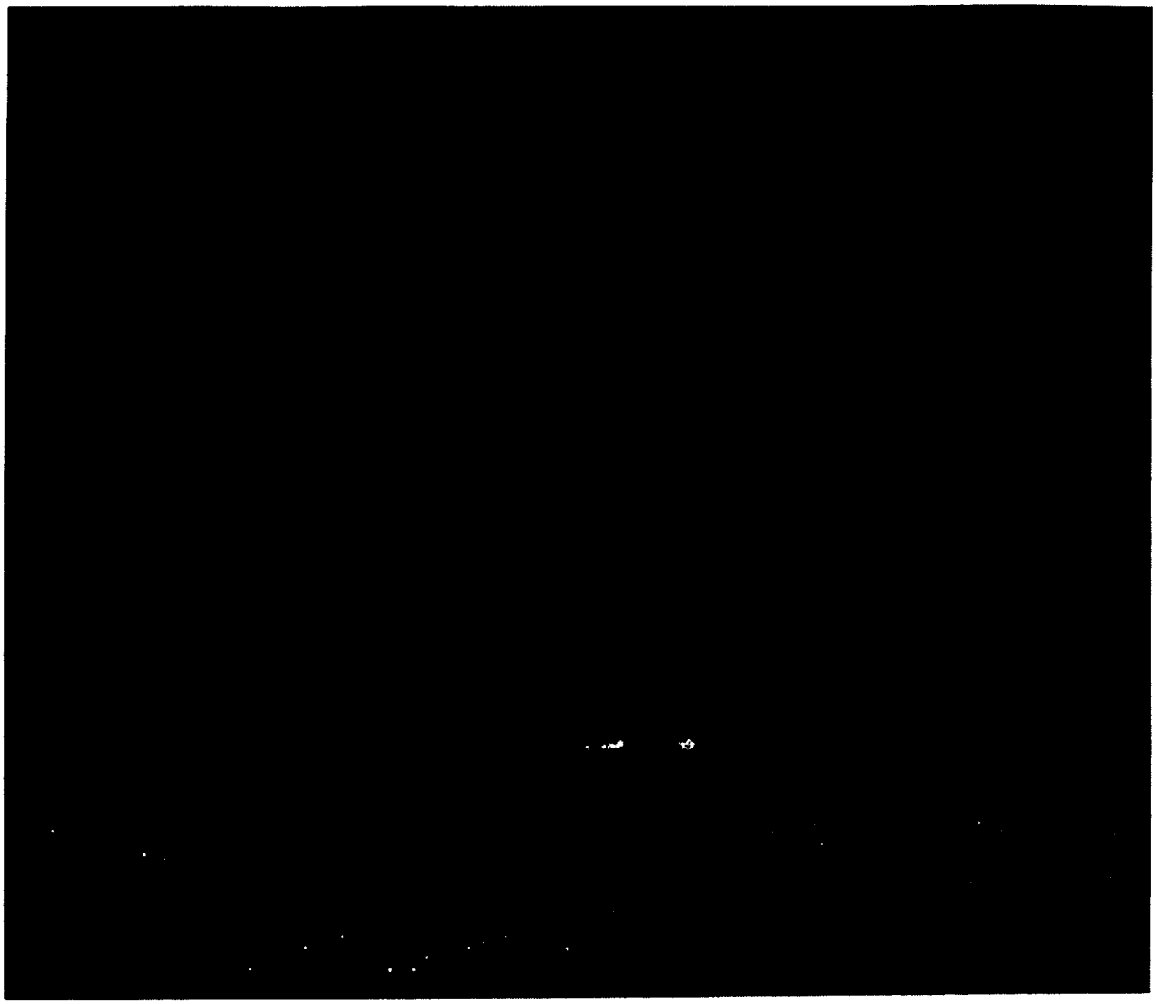

Fig. 11a.

Fig. 11. Magellan image (a) and geologic sketch map (b) of a portion of Site #22, south of the crater Yablochkina (48.28°N, 195.30°E, C1-MIDR 45N202;1). This image is part of F-MIDR 40N194; 1. Refer to Figure 3a for legend. Orientation of ridges in Pwr and fractures and ridges within Pfr are not shown in order to emphasize the location and orientation of fractures (F) radiating away from the arachnoid. Dotted and dashed lines surround distinctive flows in Pwr just west of the arachnoid.

wall and rim material, but that they are not seen for one or more of the following reasons: 1) material properties differences (solid rock versus fragmental ejecta) mean that the faults are not clearly formed or manifested in the wall and rim, 2) post-faulting mass wasting of fragmental material obscures the fractures, 3) enhanced roughness and lack of radar backscatter contrast makes detectability difficult. In any case, the observations of the Martinez crater relationships provide a cautionary note in terms of dating post-crater events. For example, if a crater floor is not characterized by a smooth floor with high radar contrast compared to surrounding units, and perhaps different material properties, it is possible that post-crater features such as rift-associated fractures could be present but not detected. For example, the crater Warren, located near Martinez (Figure 8) has such an interior, and lacks evidence of post-crater rift-associated fractures; however, on the basis of this discussion, it is not possible to rule out their occurrence with complete

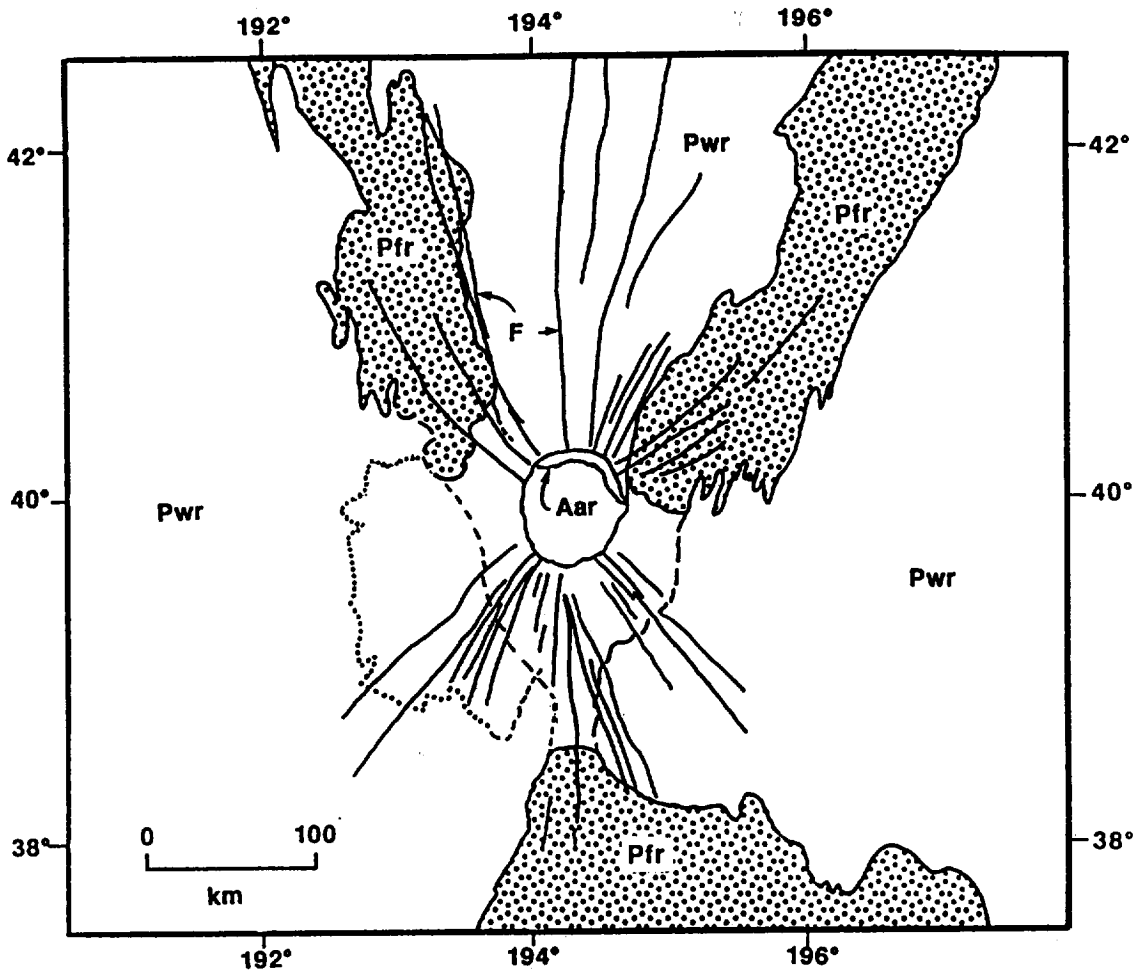

Fig. 11b.

confidence. We urge the use of stereo imaging to examine these relationships (e.g., Plaut, 1993) where such data are available.

4. Stratigraphic Relations Between Sites

On the basis of similar mapping and stratigraphic and structural analyses for all of the 36 sites, we compiled individual geologic columns for each of them (Table III). Examination and comparison of these columns permit the assessment of the sequence of events and the extent of development of these units and structures over the surface of Venus. On the basis of this comparison, we find that tessera terrain (Tt) is present in 23 of the 36 sites, and in all of these it is the most ancient terrain (see Figures 4, 5). In all 23 sites the tessera is embayed by plains with wrinkle ridges (Pwr). In 22 of these 23 sites the densely fractured terrains are also present as remnants among the plains (Pdf) or as the most ancient components of coronae (COdf). In 21 of these 23 sites, Pdf is in contact with tessera and the fracture swarms enter from Pdf into tessera and disrupt it. Therefore, the fractures of Pdf

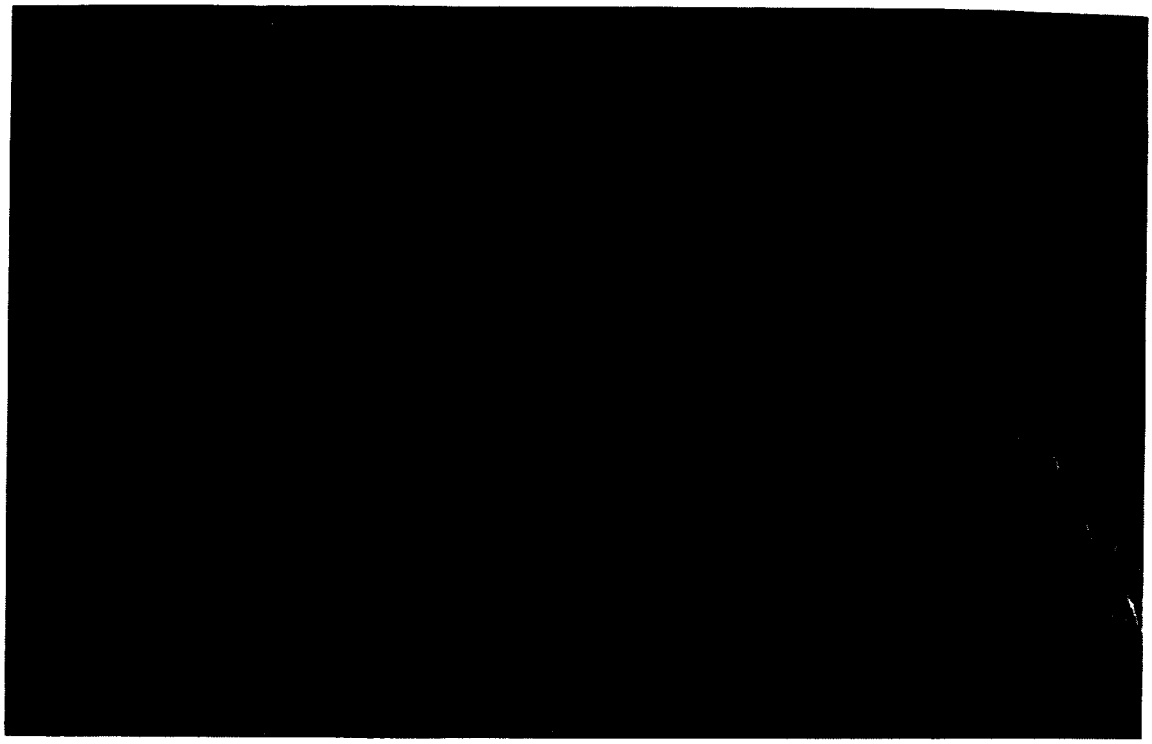

Fig. 12a.

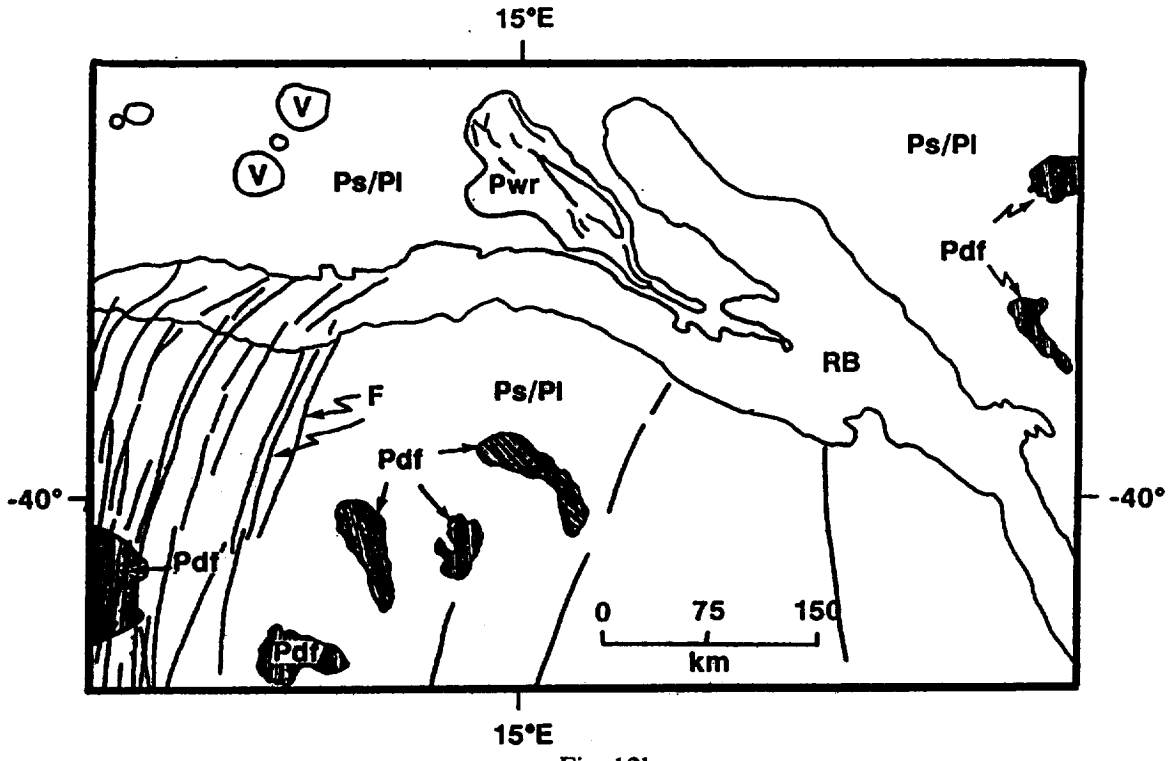

Fig. 12b.

Fig. 12. Magellan image (a) and geologic sketch map (b) of a portion of Site #2, the crater Holiday (46.73°S, 12.83°E, C1-45S011;1). Ridge belts and their relationships to surrounding units are well-illustrated in this section of C1-MIDR 45S011;201. Refer to Figure 3a for legend. Circular features are small volcanoes. The ridge belt structure is outlined and designated RB. Smooth and lobate plains occur intimately intermixed so no pattern is used in this map and the combined unit is designated Ps/Pl.

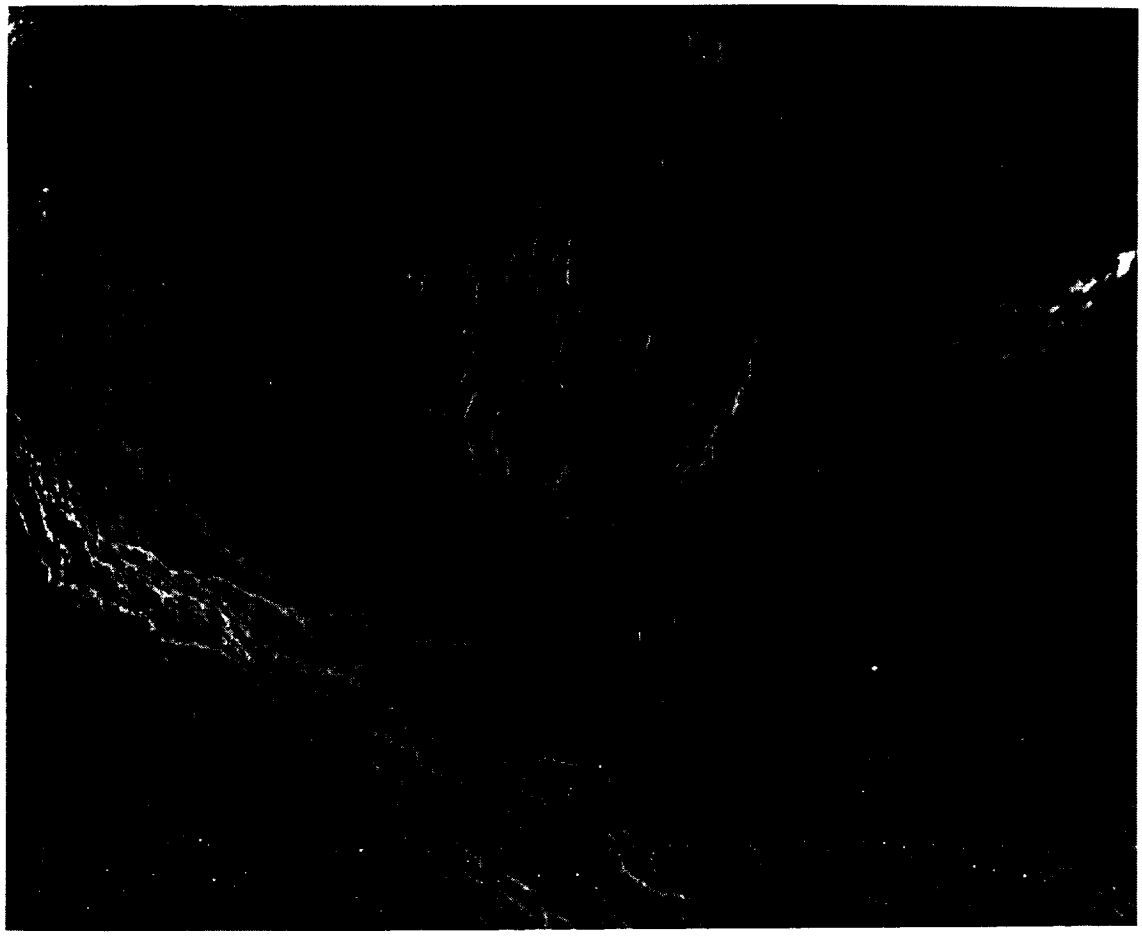

Fig. 13a.

Fig. 13. Magellan image (a) and geologic sketch map (b) of a portion of Site #1, the crater Annia Faustina (22.09°N, 4.69°E; C2-MIDR 30N026;1). Rift-associated fractures (mapped here as individual fractures, but enclosed by lines to show extent of rift zone) and their relationships to units which they cut and surrounding units are seen in the Western Eistla region SE of Gula Mons. Refer to Figure 3a for legend.

are definitely younger than tessera. The relationship between the Pdf precursor terrain and tessera is not so obvious because we did not observe the precursor terrain in an unfractured state. However, if we remove the fractures of the Pdf, the underlying terrain appears to be plains. Where Pdf is in contact with tessera it occupies local topographic lows while tessera occupies topographic highs. We may suppose, but not prove, that the precursor terrain for Pdf was plains which embayed tessera and later on the plains and partly the tessera were severely fractured with a km-scale spacing.

Densely fractured terrains forming remnants among the plains (Pdf) are often seen as fracture belts connecting coronae and merging into densely fractured terrains inside many coronae (CODf). Pdf and CODf seem to be contemporaneous and formed in a related way. Both Pdf and CODf are embayed by plains with wrinkle ridges (see Figure 6). Fractured and ridged plains (Pfr) is another type of terrain

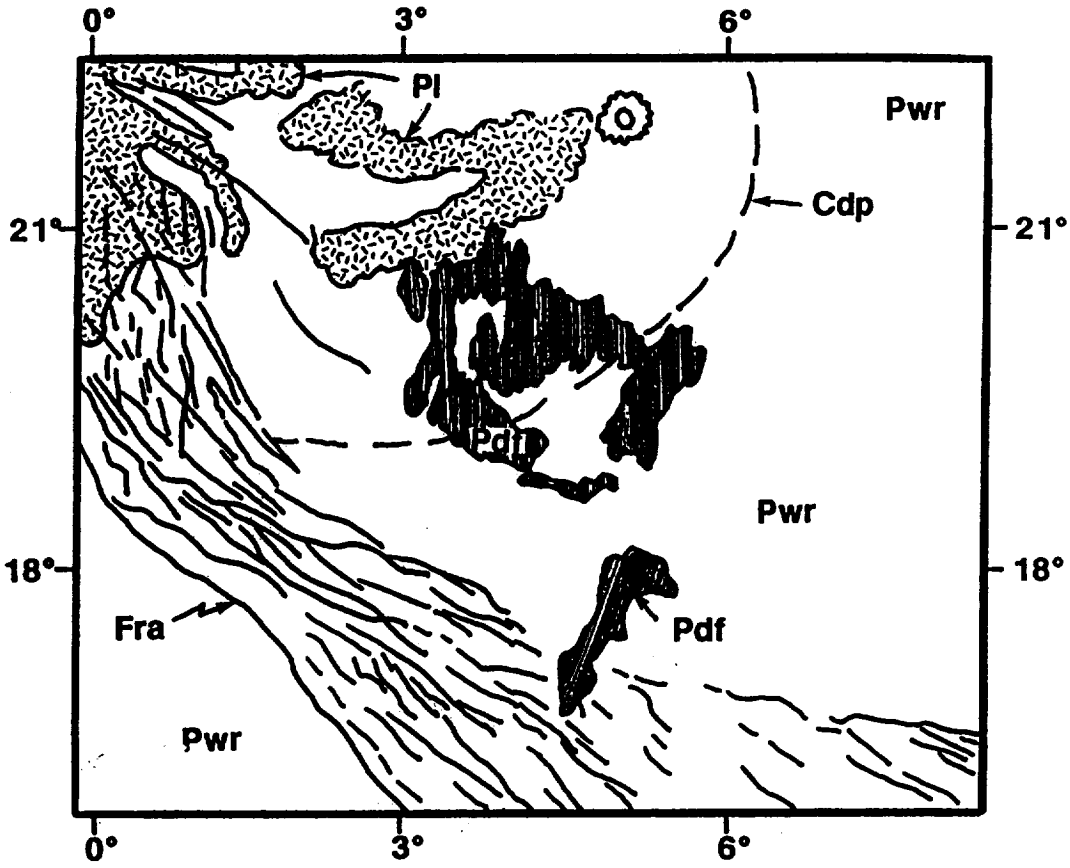

Fig. 13b.

embayed by plains with wrinkle ridges. They are usually observed as elongated remnants among Pwr and contain, in turn, in some places, remnants of Pdf within them. This determines their stratigraphic position: Pfr postdates Pdf and COdf, and predates Pwr. The ridge belt (RB) described in site #2 (see Figure 12) and site #24 (Figure 7) is morphologically very similar to ridge belts of Pfr and has the same stratigraphic position: it contains remnants of Pdf and is embayed by Pwr. Therefore, we consider RB as a probable variation of Pfr, but with a more prominent structural aspect.

Plains with wrinkle ridges (Pwr) consist of two major components: plains, and wrinkle ridges which resulted from deformation of the plains. Sometimes it is possible to see that the wrinkle ridges enter from Pwr plains into the older plains embayed by Pwr. Where Pwr are in contact with Pfr or ridge belts (RB) the wrinkle ridges are usually in structural alignment with ridges of Pfr. This implies that the ridge-forming stress orientation during these two episodes was, evidently, quite similar. When Pwr is in contact with densely fractured terrains (Pdf and COdf) or tessera (Tt) the wrinkle ridges do not enter into these terrains evidently because the highly fragmented materials composing these terrains cannot be deformed into fine-scaled wrinkle ridges and the deformation is simply distributed into small-scale movements within the unit.

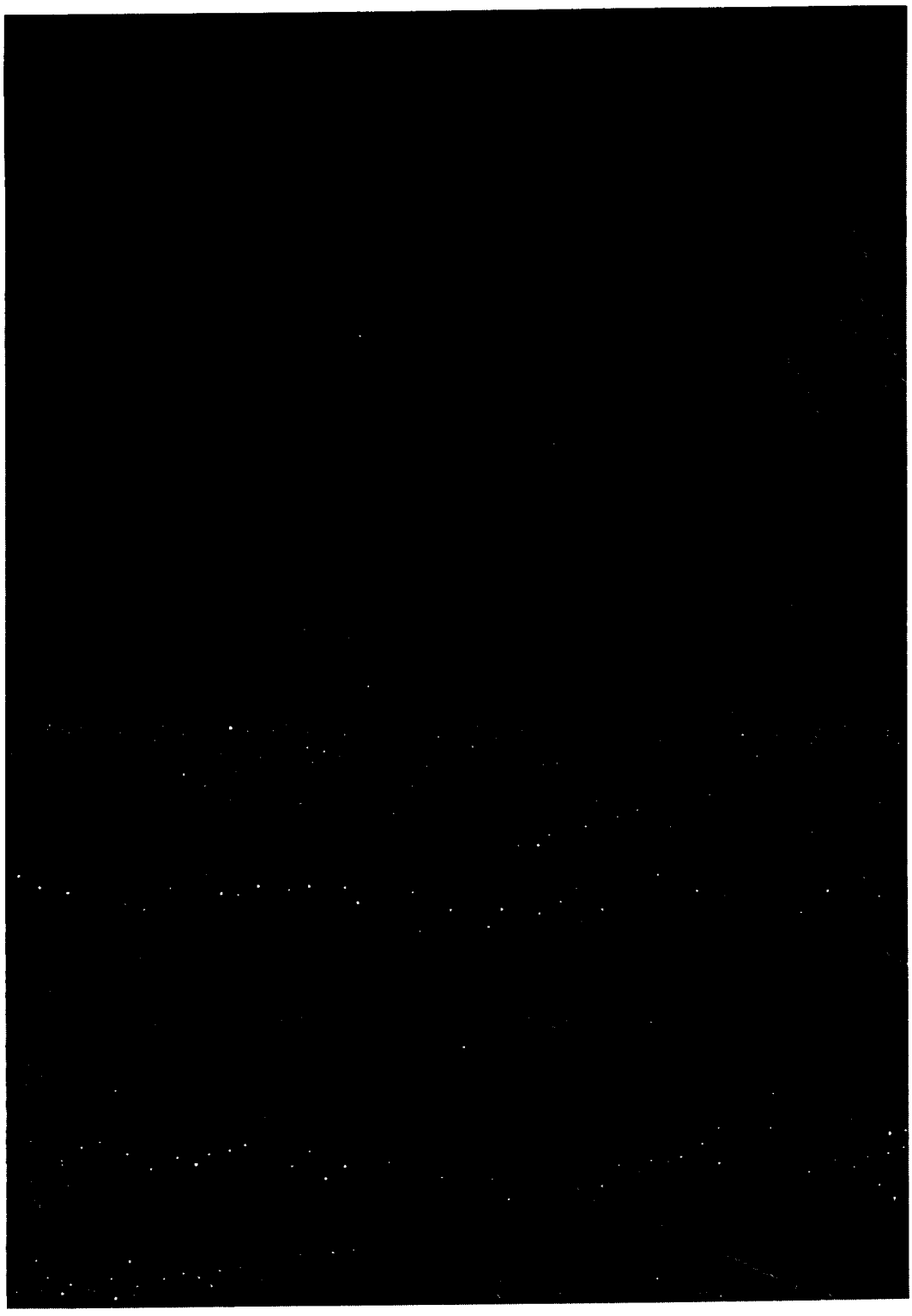

Fig. 14a.

Fig. 14. Magellan image (a) and geologic sketch map (b) of a portion of Site #13, the crater Yonge in Virava Chasma (13.96°S, 115.06°E). The interrelationship of a young crater and rift-associated fractures in plains is illustrated, using part of F-MIDR 15S117; 201. Refer to Figure 3a for legend. Yonge and its deposits and structures (rim, floor, peaks) are outlined and the lobate ejecta extending NW and N is shown as an extension of some of the deposits beyond the dashed line. Individual trends of the abundant rift-associated fractures are not shown to preserve clarity, and their location is indicated by the designation Fra.

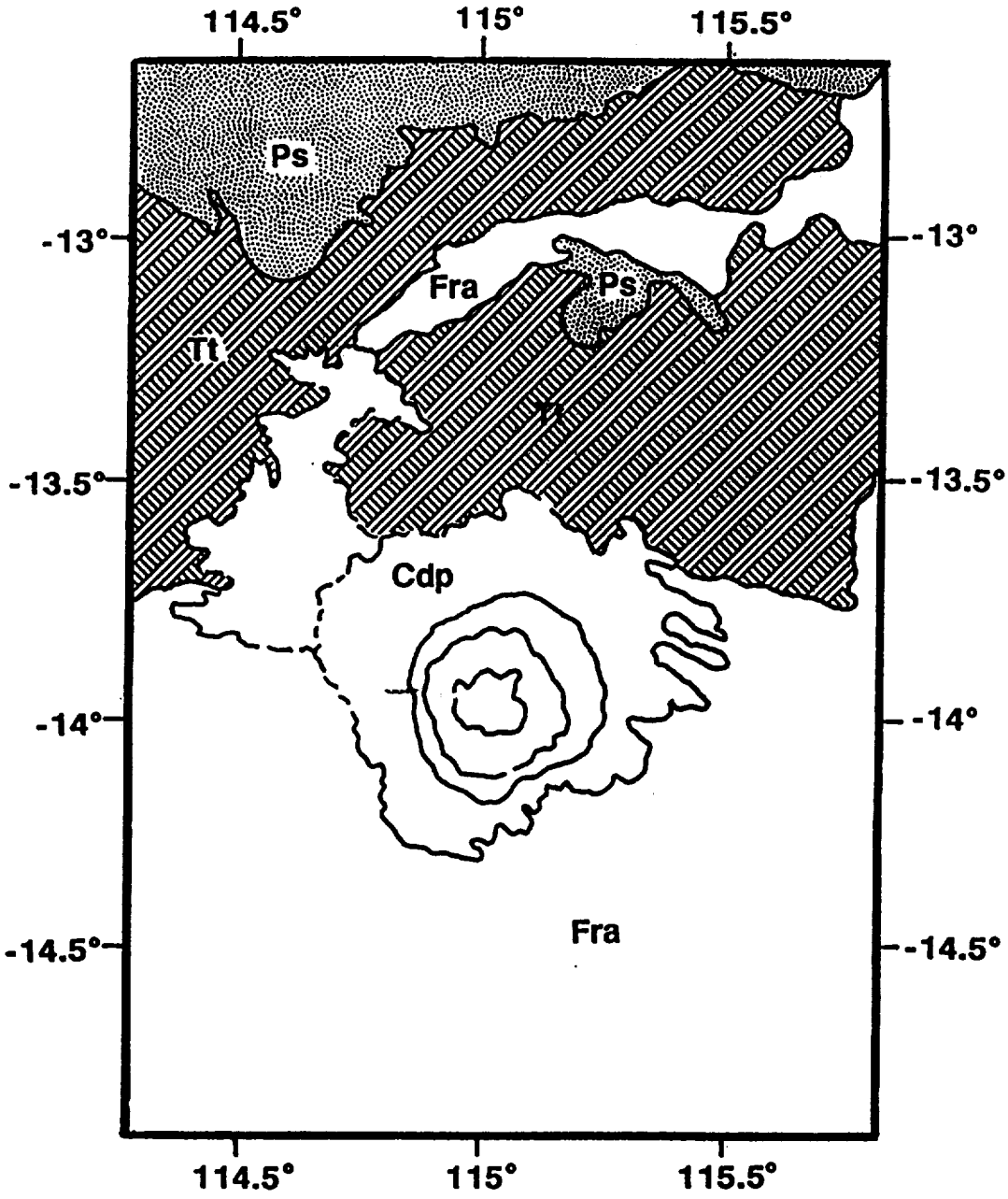

Fig. 14b.

Structural alignment is also typical for wrinkle ridges near ridges outlining arachnoids and ridges of corona annuli (see Figures 8, 9, 11). We consider this as evidence that all these ridges in a given area were formed at the same period of time. For arachnoids it is obvious, because ridges outlining them are just a part of the regional network of wrinkle ridges. For ridges of corona annuli, their formation before, and thus independently of the wrinkle ridges, seems to imply a circular symmetry and formation of complete or almost complete circular ringed rims. However, the ridges of corona annuli in the study sites never form complete circles. They are present only at some segments of the annuli, evidently those which

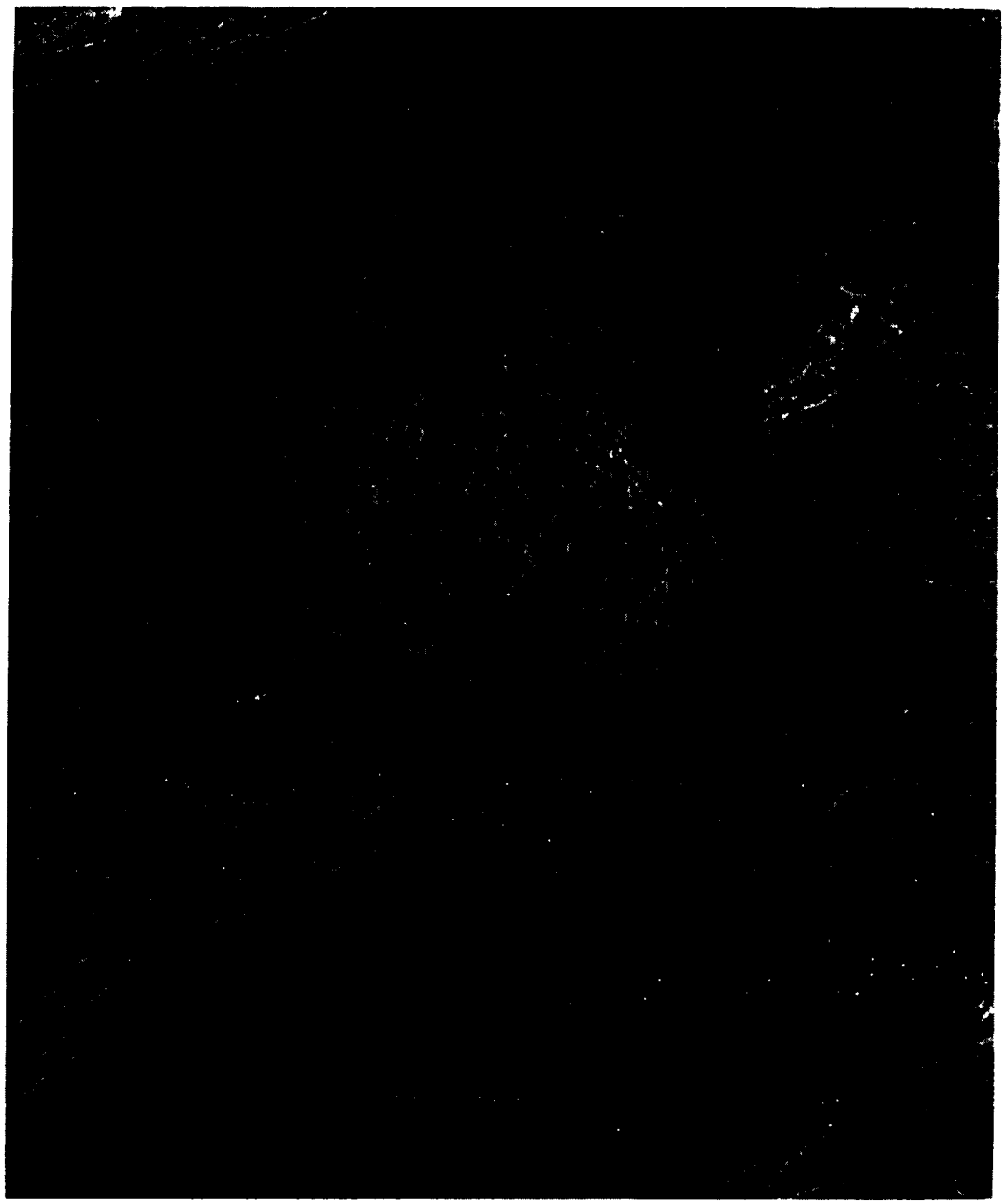

Fig. 15a.

Fig. 15. Magellan image (a) and geologic sketch map (b) of a portion of Site #20 (the crater Martinez, 11.64°S, 174.75°E, C1-MIDR 15S180;1, C1-MIDR 15S163;1). The interrelationship of a young crater and post-crater smooth plains (Ps) and rift-associated fractures (Fra) is illustrated, using part of F-MIDR 10S177;1. Refer to Figure 3a for legend. Individual trends of the abundant rift-associated fractures are not shown to preserve clarity except in the floor of Martinez, and their location is indicated by the designation Fra.

were in favorable orientation to the regional stress forming the wrinkle ridges. The alternative explanation that ridges of corona annuli were formed after the wrinkle ridges implies the involvement of wrinkle-ridged plains into the formation of the corona annuli ridges. The latter are, as a rule, more prominent than the wrinkle

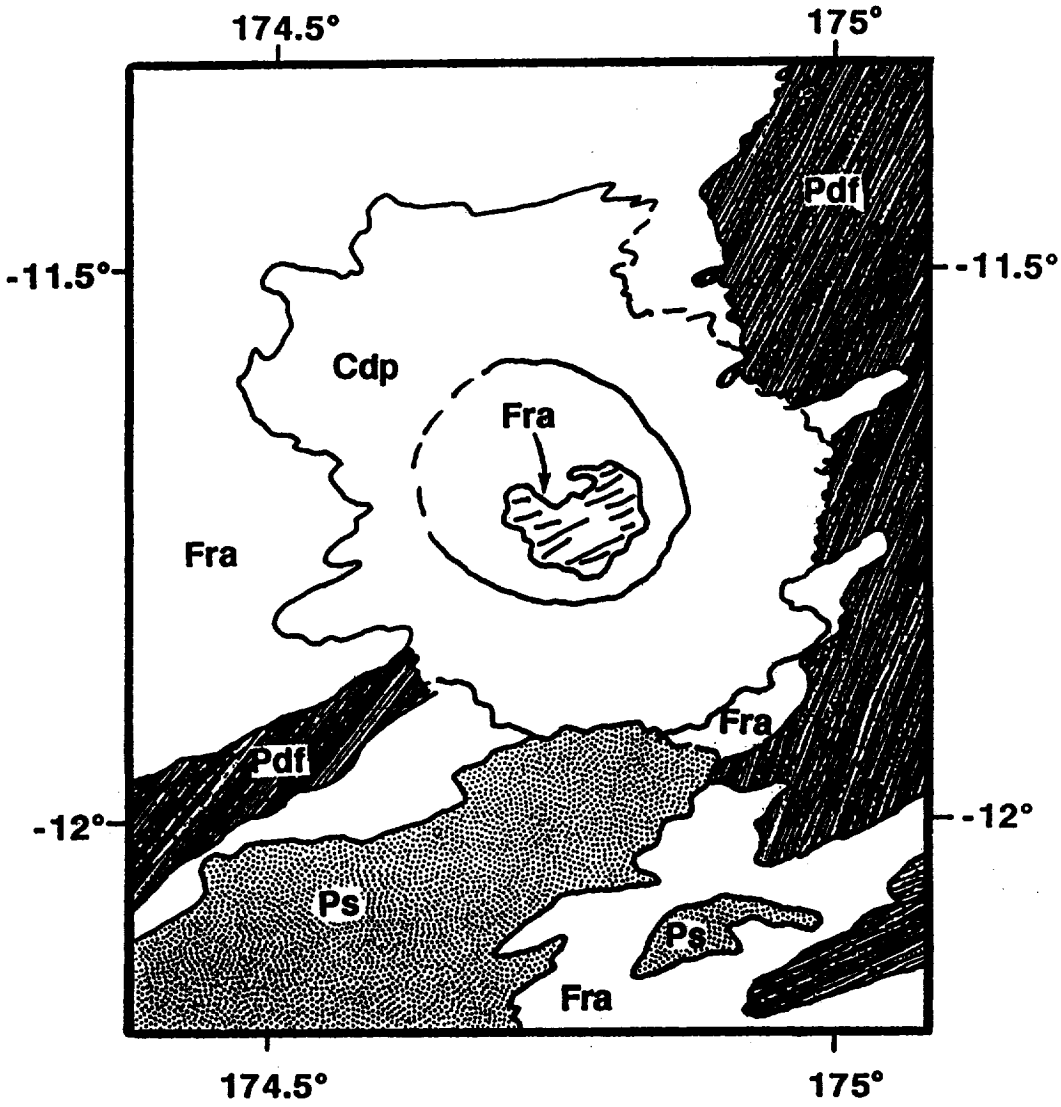

Fig. 15b.

ridges and could hardly be controlled in their formation by more faint wrinkle ridges. If this later formation of corona ridges was the case, we should observe cross-cutting relations between the corona ridges and wrinkle ridges rather than structural alignment, which is the most typical indeed.

Smooth plains (Ps) and lobate plains (Pl) are observed in 25 of the 36 sites. In most cases they show obvious superposition on plains with wrinkle ridges (see Figures 8–10, 13). In those rare cases when they are not in contact with Pwr, their stratigraphic position relative to Pwr was noted with a query; the absence of wrinkle ridges on the plains in these cases may indicate that these plains postdate Pwr, but it is not conclusive evidence.

Fractures of corona annulus (COaf) were identified in only three of the 36 sites. In two sites (#19 and 26; see Figure 10) they postdate Pwr and predate Ps. In one site (#2) they postdate Ps and predate long fractures of regional significance. Fractures

(F) were distinguished as separate structures (or collection of structures) when they disrupt Pwr and formations postdating Pwr (see Figures 10–12). Such a situation was observed in 24 sites. In formations predating Pwr, including tessera, Pdf/COdf and Pfr, fractures are the attributes of the formations and are not considered as separate structures. In 11 sites the fractures are the only structures postdating Pwr. In 13 sites they are present together with other post-Pwr formations, mostly Ps and Pl. In these cases they are also often the youngest endogenic features of the area.

Rift-associated fractures (Fra) are structures observed in 10 of the 36 sites. They and the lava flows associated with those rifts are the youngest features of endogenic origin at the sites studied. In three of those 10 sites rift-associated fractures even postdate dark-paraboloid craters (#20, Dali Chasma, see Figure 15; #23, junction of Dali, Ganis and Parga Chasmata; #25, Hecate Chasma). In one of these three sites (#23) the youngest rift-associated fractures are overlapped by lava flows of Maat Mons volcano. At site #36 the youngest rift-associated fractures apparently postdate the dark-paraboloid crater, but the evidence for that is indirect. In the other six sites (#1, 13-see Figure 13, 14) rift-associated fractures predate the dark-paraboloid craters.

Dark-paraboloid craters (Cdp) have important stratigraphic significance because we know not only that they are the youngest impact craters on Venus (Campbell *et al.*, 1992) but how young they are (<50 m.y., Basilevsky, 1993; Strom, 1993). Among 36 Cdp studied by us, paraboloids associated with 21 craters are degraded with formation of wind streaks (Ss) and reblown by wind accumulations of radar-dark debris (Sp). These 21 craters possibly represent the older part of this very young crater subpopulation.

5. The Global Geologic History Model

The relationships described above within and between the different locations and geologic columns may be summarized in the form of a generalized model of the stratigraphic sequence and geological history. This column is presented in Figure 16, where the left column shows the time sequence of units and structures, the central columns show the schematic geologic history and events which formed these units and the right column shows the interpretation of the processes that are responsible for these events. Examination of Figure 16 shows the following general themes.

A period of early intense deformation formed the tessera (Tt). The earliest deformation observed within the tessera is largely compressional, and the later is extensional (Bindschadler and Head, 1991; Bindschadler *et al.*, 1992; Ivanov and Head, 1994). There is no information from our analyses that allows us to determine if the formation of the tessera was catastrophic (e.g., Schaber *et al.*, 1992; Head *et al.*, 1993), or gradual (e.g., Solomon, 1993). However, the analysis

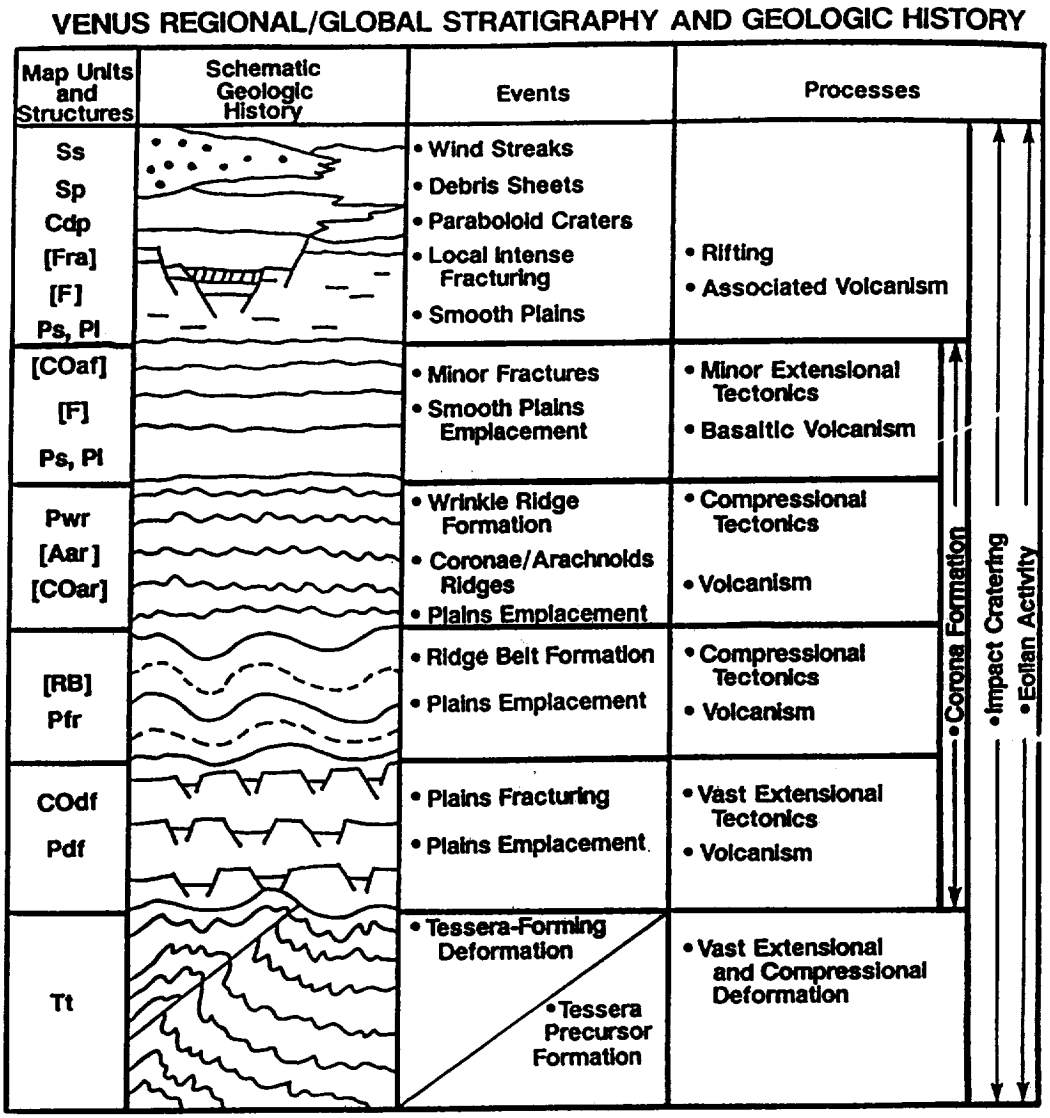

Fig. 16. Summary of Venus regional and global stratigraphy and geologic history. In the left column, map units are listed in order of stratigraphic position with oldest at the bottom, and structures are indicated in brackets in their interpreted stratigraphic position (see text for detailed description and Figure 2 for photographic examples). Interpreted geologic history is diagramatically shown in the next column. In the two right-hand columns, the events and the interpreted processes that formed them are shown. This generalized geological column was compiled on the basis of the results of analyses and interpretation in the 36 sites.

of Ivanov and Basilevsky (1993) shows that most of the large craters found on the tessera are undeformed, and thus the tessera appears not to have been tectonically active throughout most of the period of the emplacement of the population of craters superposed on the tessera. This contradicts the predictions of the gradual deformation option and favors the catastrophic option.

Following, and indeed coincident with the terminal stages of tessera formation, plains units formed and then were heavily deformed by a very dense pattern of closely spaced fractures and graben (Pdf). This unit appears to be very widespread

and the density of these is much higher, while spacing is much less, than later on (e.g., the rift-associated fractures, Fra), providing some evidence for the thermal state of the lithosphere at the time (e.g., thinner at this time than later). This phase of extensional deformation seems to be related to the latter stages of extensional deformation observed on the tessera because often the graben and fractures are parallel to and continue into those in the tessera.

The emplacement of volcanic plains continued, but deformation of the plains switches from extensional (Pdf) to compressional, as evidenced by the formation of broad ridges in Pfr, ridge belts (RB), and plains with wrinkle ridges (Pwr). In many cases (e.g., Lavinia Planitia; Squyres *et al.*, 1992), regional ridge belts formed early in this period, prior to the formation of regional ridged plains (Pwr). There is often clear evidence for the formation of ridge belts from volcanic plains, followed by the subsequent embayment by volcanic plains which have the regional, much smaller-scale wrinkle ridges. The widespread nature of these plains with wrinkle ridges indicates that this may be a near-global phenomena. In some cases, Pwr shows two directions of wrinkle ridge orientation at large angles to one another and in sequence. This has been interpreted to mean that the orientation of maximum principle stresses changed considerably at least locally during the period of wrinkle ridge formation (e.g., McGill, 1993). On a larger scale, however, the global distribution and orientation of ridges in ridged plains suggests a broad-scale global control linked to the major equatorial topography, not just local smaller-scale regions (Bilotti *et al.*, 1993).

The general change from extensional to compressional deformation in the plains would seem to support the idea of a general cooling and thickening of the lithosphere, although detailed mapping and correlation is required in order to distinguish between a global event or trend and the simple local emplacement of plains units, loading of the lithosphere, subsidence, and compressional deformation to produce the wrinkle ridges. Similarly, evidence in the areas we examined points to the early formation of many of the large ridge belts, followed by ridged plains emplacement. Is this a major phase in the history of Venus comparable to that of tessera formation?

At the present time, deformation is regionally extensional and is displayed in the form of rift-associated fractures (Fra) and local fractures/graben (F). Stratigraphic superposition shows that smooth plains have recently been emplaced and these units show evidence for specific lobate forms and sources (Pl), or more commonly, are smooth to mottled (Ps); in the latter unit, individual flows and sources cannot be readily identified for any length. Do these patterns represent local to regional extensional deformation caused by regional uplift (Beta, Atla), or are they the result of a net state of extension in the lithosphere? For example, are the smooth plains not deforming to ridged plains because the state of stress in the lithosphere is generally extensional? Or is the state of stress generally compressional, but the smooth plains have simply not deformed yet because they are young and the rifting simply indicates local uplift and extension?

6. Synchronous vs. Nonsynchronous Options

The major question which arises from the stratigraphic correlation model is 1) whether the same stratigraphic units and the corresponding geologic events were generally synchronous in all the sites or 2) whether this sequence is just a typical sequence of events which occurred in different places at different times. The first option means that the proposed stratigraphic correlation model describes a sequence of events which is a part of the global geologic history of Venus. The second option means that a typical characteristic of the geologic history of Venus is the multiple repetition of the same scenario in different places at different times, a kind of local sequence or cycle of tectonism and magmatism.

This dilemma is actually just another view of the current discussion on the character of the geologic history of Venus. The extreme opinions in this discussion are represented by the papers of Schaber *et al.* (1992) and Phillips *et al.* (1992). Both of them try to explain the basic observation that, first, most of the observed impact craters on Venus have a pristine appearance and do not look embayed by the surrounding volcanic plains but rather are superposed on them, and second, that the crater areal distribution around the planet is not distinguishable from a random one. Schaber *et al.* (1992) believe that the observed crater population is a production population. In that case the crater retention age of the venusian surface is estimated to be about 500 m.y. This means that about 500 m.y. ago the surface of Venus was catastrophically flooded by extensive volcanic eruptions which destroyed the pre-existing crater population. Following this event, the volcanic and tectonic activity on Venus was minor and continued bombardment formed the observed population in a randomly distributed manner; the impact craters were mostly not affected by volcanism.

Parmentier and Hess (1992) and Head *et al.* (1994) suggested that this catastrophic flooding might be caused by gravitational instability originating from melting out basalts from the upper mantle of the planet; this supposedly should lead to the situation where geochemically depleted and cold material of the upper mantle came to be more dense than the hot and fertile material lower in the mantle. It should lead to major overturn and result in the massive melting out of basaltic magmas from the uplifted and thus decompressed and overheated material from lower in the mantle. This model proposed by these authors also accounts for the formation of tessera terrain (Head *et al.*, 1994) which is considered by them to be the result of this overturn, and caused by large-scale deformation of the crust accompanying the event. This option agrees with our first option that the observed stratigraphic sequence was formed by the sequence of geologic events which were almost synchronous all around the planet.

Phillips *et al.* (1992) based their model on the same facts: that the majority of the observed craters are not embayed by the surrounding volcanic plains and that the areal distribution of craters is not distinguishable from a random one. But opposite to Schaber *et al.* (1992), Phillips *et al.* (1992) consider this crater population not as

a production one but as an equilibrium one. They believe that the global thermal cataclysm was not the case and that the observed situation might be the result of permanent endogenic activity of Venus which occurred in the form of active zones of limited size in different places around the planet at different times. They estimated that their model may correspond to the observed characteristics of the crater population if these active zones were about 400 km across. In their model the average crater retention age of the Venus surface is about 700 m.y. The model of Phillips *et al.* (1992) agrees with our second option that the observed stratigraphic sequence simply reflects a typical sequence of geologic events which occurred in different places at different times.

Our observations on the stratigraphic relations of terrains and features in the 36 studied areas can help to make a choice between the discussed options and a key parameter for that is the size of the zones of endogenic activity estimated by Phillips *et al.* (1992). Indeed within any of these zones the volcanic and tectonic events of this given activity cycle certainly might form the observed stratigraphic sequence. But on the boundaries of this given activity zone where it neighbors another zone in which activity occurred at a different time, we should observe a superposition of two regional stratigraphic sequences. We would see this in the form of a variation from the typical sequence when, for example, the stratigraphically lower units, such as tessera or densely fractured terrains of the younger cycle were superimposed on the upper units, such as plains with wrinkle ridges, smooth or lobate plains, of the older cycle.

The typical size of the active zones estimated by Phillips *et al.* (1992) is about 400 km across. This is significantly less than the size of our study areas (1000 $\times$ 1000 km). This means that within each of our study areas we should have several of these active zones. So if the model of Phillips *et al.* (1992) is correct, we certainly should observe the previously mentioned superpositions of regional stratigraphy expressed in the form of violations of the typical stratigraphic sequence. But we do not observe this in any of the 36 areas. This means evidently that the hypothesis that the supposed regional activity occurred in different places at different times is unlikely to be the dominant case, and appears to favor the idea that major geologic events reflected in the stratigraphic sequence were almost synchronous and planetwide. Unfortunately this conclusion is a model-dependent one because we tried to find the solution testing the results of calculations made by Phillips *et al.* (1992). In the following discussion we address this problem using another approach.

The uppermost or nearly uppermost units of all the studied sites are dark-paraboloid craters. They represent the youngest 10% of the Venus crater population (Campbell *et al.*, 1992). Therefore, with the accuracy of 10% of the time of accumulation of the Venus crater population (about 50 m.y.) we may consider this stratigraphic unit as approximately synchronous all over the planet.

The lowermost unit at the majority of the sites is tessera. Crater density counts show that tessera on the average is older than the plains as a whole; the difference

TABLE V

Crater Densities (per 10^6 km^2) in Tessera (Areas from Ivanov and Head, 1993, in press)

Tessera	Area, 10^6 km^2	Number of Craters	Density	Standard	Range
Ovda	9.07	22	2.42×10^{-6}	0.52×10^{-6}	$1.90–2.94 \times 10^{-6}$
Fortuna	3.23	5	1.55×10^{-6}	0.69×10^{-6}	$0.86–2.24 \times 10^{-6}$
Tellus	2.46	4	1.63×10^{-6}	0.81×10^{-6}	$0.82–2.44 \times 10^{-6}$
Thetis	2.26	5	2.22×10^{-6}	0.99×10^{-6}	$1.23–3.21 \times 10^{-6}$
Phoebe	1.22	4	3.28×10^{-6}	1.64×10^{-6}	$1.64–4.92 \times 10^{-6}$
All Tesserae	37.00	76	2.05×10^{-6}	0.36×10^{-6}	$1.69–2.41 \times 10^{-6}$

in age may not be large but it is statistically reliable. If the average age of plains is about 500 m.y. [more recently revised to about 288 (+311, −98) m.y. by Strom *et al.*, 1994], the tessera average age is estimated as 700 + 265/−195 m.y. (Ivanov and Basilevsky, 1993). The crater distribution among the largest blocks of tessera is shown in Table V. The data given in Table V show that the crater density of five of the largest tesserae vary within a factor of 1.6 from the average density for all tesserae of Venus and all the differences are not statistically reliable. Therefore, at least for the largest tessera blocks, there is no reliable evidence that they are different in age from each other and this favors the option of global synchroneity of this major stratigraphic unit.

But even if tessera-forming events and the dark-paraboloid craters on Venus were globally approximately synchronous it does not mean that in the intervening part of the stratigraphic sequence the major units were also synchronous. The most crucial issue for this hypothesis of global synchroneity of major stratigraphic units is the problem of whether the wrinkle ridges on venusian plains are approximately contemporaneous or not. If the observed stratigraphic sequence was just a typical scenario realized in different places of Venus at different times (e.g., the wrinkle ridges form due to loading and subsidence after the emplacement of plains units) we would expect that in some places this typical sequence of events will be realized at least twice. Tne consequence of such superposition might be the presence of plains part of which were deformed by wrinkle ridges once (in a new event) and another part, twice (in a new and old event). Although situations are observed in which two distinct directions of wrinkle ridges occur in one plains unit (McGill, 1993), the global distribution and orientation of wrinkle ridges seems to be very sweeping and systematic (Bilotti *et al.*, 1993) and to suggest regional to global, rather than completely local, control. In addition, Schaber *et al.* (1992) noted that of all the impact craters examined on 89% of the surface of Venus, only one was deformed by compressional structures (class c, Barrymore crater, 52.3°N, 195.6°E). This appears to strongly support the idea that the volcanic plains and their associated

wrinkle ridges were formed early, and in a short period of time. Future observations as part of the Venus Data Analysis Mapping Program will help to test such ideas and will fill in much of the intervening areas between these 36 sites in order to assess the global significance of this preliminary geologic sequence (Figure 16).

7. Summary and Conclusions

In this study we have shown that major mappable stratigraphic units and structures can be identified on Venus and that these can be mapped successfully in large regions ($\sim 10^6$ km^2) over the whole planet. Such studies in 36 randomly distributed regions show evidence for a distinctive regional and global geological sequence. This sequence in turn provides evidence for a model of geological history that highlights several major themes in the history of Venus.

On the basis of this analysis, we favor a model in which most of the history of Venus (that of its first 80% or so) is not preserved in the surface geomorphological record. Whatever record that existed in the past (heavily cratered surfaces, etc.) seems to have been destroyed prior to or by the major deformation associated with tessera formation in the period between 0.5–1.0 b.y. ago (Ivanov and Basilevsky, 1993). Such intense levels of regional deformation as those associated with the tessera are not observed again in the subsequent history of Venus. Our stratigraphic analysis supports the idea (Ivanov and Head, 1994) that tessera extends underneath at least twice as much of the surface as is observed in its presently exposed area. On the basis of the difference in intensity and style of deformation between tessera formation and later deformation as observed in our study, and the evidence that most of the deformation occurred in the period prior to about 500 m.y. ago (Ivanov and Basilevsky, 1993), we favor a hypothesis that relates tessera formation to a relatively "catastrophic" event (e.g., Schaber *et al.*, 1992; Parmentier and Hess, 1992), rather than as a normal consequence of the general thermal evolution of Venus (e.g., Solomon *et al.*, 1993).

In the terminal stages of tessera formation, extensive parallel linear graben swarms were formed on the tessera and on the volcanic plains that were emplaced up to that time. These features are often responsible for the typical orthogonal pattern that characterizes the tessera fabric. It is clear that they represent a change in the style of deformation of the tessera terrain from shortening to extension. The cause of this change could be related to gravitational relaxation of the newly deformed tessera (e.g., Bindschadler *et al.*, 1992). Alternatively, if the tessera formed from the catastrophic loss of a depleted mantle layer (e.g., Parmentier and Hess, 1992), graben formation could result from the ascent of hot, fertile mantle material to shallower depths, its pressure-release melting, and the resulting change to a net state of extension in the shallow parts of the planetary interior.

Following the formation of tessera, extensive volcanic flooding resurfaced at least 85% of the planet. On the basis of the characteristics of impact crater flooding

(a very small percentage of impact craters are embayed by volcanic flows), Schaber *et al.* (1992) have proposed that the emplacement of plains was relatively rapid and that subsequent formation of volcanic plains was minimal. This hypothesis is supported by Monte Carlo simulations of flooding and impact cratering (Bullock *et al.*, 1993). Our stratigraphic analysis suggests that the ridged plains correspond to the period in which the majority of volcanic resurfacing occurred. Evidence from our analysis that favors a high flux in the post-tessera period includes the formation of extensive sinuous channels in the plains prior to the formation of the wrinkle ridges on them. This suggests that the style of emplacement of the ridged plains involved the formation of these hundreds to thousands of km long channels, features which are not seen on later flow units. At present, we have no conclusive evidence for the duration or the absolute age of the ridged plains emplacement and deformation, although the observation of Schaber *et al.* (1992) that only one crater in the total population examined has been modified by compressional deformation suggests that it is likely to have been early and over a relatively short period.

During the emplacement of the post-tessera and post-fractured plains units, the net state of stress in the lithosphere apparently changed from extensional to compressional, first in the form of extensive ridge belt development (e.g., Lavinia Planitia), and then followed by the formation of extensive wrinkle ridges on the flow units. This was then followed by local emplacement of smooth plains units which often emanate from individual sources and which are essentially undeformed. The size and distribution of these (Head *et al.*, 1992; Crumpler *et al.*, 1993) indicates that they are not contributing to resurfacing in a major way.

Although we cannot rule out the local nature of the formation of ridged plains (see previous discussion), we are struck by the similarities between this sequence on Venus and the sequence of events in the tectonic and volcanic history of the Moon. On the Moon, early extensive radioactive heating and melting following the formation of the anorthosite crust continued to keep the lunar lithosphere in a net state of extension, favoring the production of mare basalt magmas, their emplacement on the surface, the loading of the mare basins, and the formation of extensional deformation features such as linear rilles (Solomon, 1978; Solomon and Head, 1980). As the lithosphere cooled and thickened, the net state of stress in the lithosphere changed from extensional to compressional, and the emplacement of volcanic plains and loading of the lithosphere resulted in downwarping and the formation of major mare ridge belts, comparable in scale to those formed on Venus. Subsequent continued global cooling and thickening of the lithosphere caused a decrease in the net global volcanic flux, and the slowing and then ultimately the cessation of surface deformation of these flows. This sequence of events (decrease in volcanic flux, change in tectonic style, and thickening of the lithosphere) is thus very similar to that observed and interpreted on Venus, although the causes are likely to have been different. We are presently analyzing the spacing of deformational features (e.g., Zuber, 1990) to see if they are consistent with the interpreted changes in the thermal structure of Venus.

On the basis of the latest part of the stratigraphic record (represented by the dark paraboloid craters which apparently formed in the last 50 million years), the major events in the last 10% of the presently preserved history of Venus are continued rifting and some minor associated volcanism, and the eolian redistribution of material largely derived from impact crater deposits. It is currently unknown whether the present state represents a normal consequence of its general thermal evolution and is representative of the level of geological activity predicted for the future, or if Venus has been characterized by a sequence of periodic global changes in the composition and thermal state of its crust and upper mantle (e.g., Parmentier and Hess, 1992) in which case, Venus could return to levels of deformation and resurfacing typical of the period of tessera formation.

Detailed geologic mapping and stratigraphic synthesis can begin to address some of the outstanding problems raised by this and other analyses, including:

- For the tessera, what is the nature of tessera precursor terrain? What is the range of models for the formation and evolution of the tectonic features and how can this information be used to decipher the implications for stress distribution and orientation?
- What is the global relationship of fractured plains and the late-stage graben in the tessera? Does global mapping support the hypothesis that they are related?
- What is the stratigraphic position and significance of Akna, Freyja, and Maxwell montes?
- Do large ridge belts form exclusively in the early wrinkle-ridged plains era if it existed as a separate time period, or are they significant throughout?
- What is the mean global volcanic output as a function of time? On the basis of the examination of regional stratigraphic relationships, the ridged plains are clearly more voluminous than the smooth and lobate plains, but what is the time interval over which each was emplaced?
- What is the exact stratigraphic timing of coronae? Are they predominantly in the post-tessera, pre-ridged plains era, or are they formed at practically the same rate throughout the sequence? Are there several different modes of origin for coronae and related features and if so, do the different modes tend to occur at different times?
- Is there any evidence for large ancient rifts?
- What is the stratigraphic position of large volcanic edifices? Do they represent a relatively late phenomenon or are they dispersed throughout the stratigraphic sequence and subsequently modified by flooding and/or gravitational relaxation so that they are not readily recognizable?

Acknowledgements and Note

We thank Elena Zabalueva for the statistical tests of the randomness of the positions of our study sites, George Burba for review of the manuscript for consistency with

International Astronomical Union nomenclature, and two anonymous reviewers for comments that improved the manuscript. Thanks are extended to Kari Magee and Kopal Jha for discussions and to the National Aeronautics and Space Administration for financial support to ATB and JWH as part of the Venus Data Analysis Program (VDAP), and to the International Science Foundation Grant M2F000 to ATB. Thanks are extended to Karen Plouff and Amy Johnson for drafting and to Peter Neivert for photographic assistance. Detailed geologic descriptions of the 36 study sites may be found in Basilevsky and Head (1994), which is available from the Brown University Library through interlibrary loan.

References

ACSN, 1961, American Code of Stratigraphic Nomenclature, *Am. Assn. Petrol. Geol. Bull.* **45**, 645–660.

Barsukov, V. L., *et al.*: 1986, 'The Geology and Geomorphology of the Venus Surface as Revealed by the Radar Images Obtained by Venera 15 and 16', *J. Geophys. Res.* **91**, D399–411.

Basilevsky, A. T.: 1993, 'Age of Rifting and Associated Volcanism in Atla, Regio, Venus', *Geophys. Res. Lett.* **20**, 883–886.

Basilevsky, A. T. and Head, J. W.: 1994, 'Characteristics of the Geology of Thirty-Six Sites on Venus', Brown University Library, Providence RI, 72 p.

Basilevsky, A. T., Pronin, A. A., Ronca, L. B., Kryuchkov, V. P., Sukhanov, A. L., and Markov, M. S.: 1986, 'Styles of Tectonic Deformations on Venus: Analysis of Venera 15 and 16 Data', *J. Geophys. Res.* **91**, suppl., D399–D411.

Bilotti, F.: 1992, 'Global Organization of Tectonic Deformation on Venus', *Lunar Planet. Sci. Conf.* **24**, 107–108.

Bindschadler, D. L. and Head, J. W.: 1991, 'Tessera Terrain, Venus: Characterization and Models for Origin and Evolution', *J. Geophys. Res.* **96**(B4), 5889–5907.

Bindschadler, D. L., Schubert, G., and Kaula, W. M.: 1992, 'Coldspots and Hotspots: Global Tectonic and Mantle Dynamics of Venus', *J. Geophys. Res.* **97**(E8), 13563–13578.

Bullock, M. A., Grinspoon, D. H., and Head, J. W.: 1993, 'Venus Resurfacing Rates: Constraints Provided by 3-D Monte Carlo Simulations', *Geophys. Res. Lett.* **20**, 2147–2150.

Campbell, D. B., Stacy, N. J. S., Newman, W. I., Arvidson, R. E., Jones, E. M., Musser, G. S., Roper, A. Y., and Schaller, C.: 1992, 'Magellan Observations of Extended Impact Crater Related Features on the Surface of Venus', *J. Geophys. Res.* **97**, 16249–16277.

Crumpler, L. S., Head, J. W., and Aubele, J. C.: 1993, 'Relation of Major Volcanic Center Concentration on Venus to Global Tectonic Patterns', *Science* **261**, 591–595.

Diggle, P. J., Fisher, N. I., and Lee, A. J.: 1985, 'A Comparison of Tests of Uniformity for Spherical Data', *Austral. J. Statistics* **27**, 53–59.

Greeley, R., Arvidson, R. E., Elachi, C., Geringer, M. A., Plaut, J. J., Saunders, R. S., Schubert, G., Stofan, E. R., Thouvenot, E. J. P., Wall, S. D., and Weitz, C. M.: 1992, 'Aeolian Features on Venus: Preliminary Magellan Results', *J. Geophys. Res.* **97**(E8), 13319–13345.

Greeley, R. and Guest, J. E.: 1987, *Geological Map of the Eastern Equatorial Region of Mars*, U.S. Geological Survey Map I-1802-B.

Head, J. W., Crumpler, L. S., Aubele, J. C., Guest, J. E., and Saunders, R. S.: 1992, 'Venus Volcanism: Classification of Volcanic Features and Structures, Associations, and Global Distribution from Magellan Data', *J. Geophys. Res.* **97**(E8), 13153–13197.

Head, J. W., Parmentier, E. M., and Hess, P. C.: 1994, 'Venus: Vertical Accretion of Crust and Depleted Mantle and Implications for Geological History and Processes', *Planetary and Space Science*, in press.

Head, J. W., Pieters, C. M., McCord, T. B., Adams, J. A., and Zisk, S.: 1978, 'Definition and Detailed Characterization of Lunar Surface Units Using Remote Observations', *Icarus* **33**, 145–172.

Ivanov, M. A. and Basilevsky, A. T.: 1993, 'Density and Morphology of Impact Craters on Tessera Terrain, Venus', *Geophys. Res. Lett.* **20**, 2579–2582.

Ivanov, M. A. and Head, J. W.: 1994, 'Tessera Terrain on Venus: A Survey of the Global Distribution, Characteristics, and Relation to Surrounding Units from Magellan Data', *Earth, Moon and Planets*, submitted.

McGill, G. E.: 1993, 'Wrinkle Ridges, Stress Domains, and Kinematics of Venusian Plains', *Geophys. Res. Lett.* **20**, 2407–2410.

Nikishin, A. M., Pronin, A. A., and Basilevsky, A. T.: 1992, in V. L. Barsukov *et al.* (eds.), *Hot-Spot Structures, in Venus Geology, Geochemistry, and Geophysics, Research Results from the USSR*, University of Arizona Press, pp. 31–67.

Parmentier, E. M. and Hess, P. C.: 1992, 'Chemical Differentiation of a Convecting Planetary Interior: Consequences for a One Plate Planet Such as Venus', *Geophys. Res. Lett.* **19**, 2015–2018.

Phillips, R., Raubertas, R. F., Arvidson, R. E., Sarkar, I. C., Herrick, R. R., Izenberg, N., and Grimm, R. E.: 1992, 'Impact Craters and Venus Resurfacing History', *J. Geophys. Res.* **97**, 15923–15948.

Plaut, J. J.: 1993, in J. P. Ford *et al.* (eds.), *Stereo Imaging, in Guide to Magellan Image Interpretation*, Chapter 4, JPL Pub., 93–24, 33–44.

Roberts, K. M., Guest, J. E., Head, J. W., and Lancaster, M. G.:1992, 'Mylitta Fluctus, Venus: Rift-Related, Centralized Volcanism and the Emplacement of Large-Volume Flow Units', *J. Geophys. Res.* **97**, 15991–16015.

Schaber, G. G., Strom, R. G., Moore, H. J., Soderblom, L. A., Kirk, R. L., Chadwick, D. J., Dawson, D. D., Gaddis, L. R., Boyce, J. M., and Russell, J.: 1992, 'Geology and Distribution of Impact Craters on Venus: What are They Telling Us?', *J. Geophys. Res.* **97**(E8), 13256–13302.

Scott, D. H. and Tanaka, K. L.: 1986, 'Geological Map of the Western Equatorial Region of Mars', U.S. Geological Survey Map I-1802-A.

Senske, D. A., Schaber, G. G., and Stofan, E. R.: 1992, 'Regional Topographic Rises on Venus: Geology of Western Eistla Regio and Comparison to Beta Regio and Atla Regio', *J. Geophys. Res.* **97**, 13395–13420.

Squyres, S. W., Jankowski, D. G., Simons, M., Solomon, S. C., Hager, B. H., and McGill, G. E.: 1992, 'Plains Tectonism on Venus: The Deformation Belts of Lavinia Planitia', *J. Geophys. Res.* **97**(E8), 13579–13599.

Solomon, S. C.: 1978, 'On Volcanism and Thermal Tectonics on One-Plate Planets', *Geophys. Res. Lett.* **5**, 461–464.

Solomon, S. C.: 1993, 'A Tectonic Resurfacing Model for Venus', *Lunar and Planetary Science Conference* **24**, 1331–1332.

Solomon, S. C. and Head, J. W.: 1980, 'Lunar Mascon Basins: Lava Filling, Tectonics and Evolution of the Lithosphere', *Reviews of Geophysics and Space Physics* **18**, 107–141.

Solomon, S. C., Smrekar, S. C., Bindschadler, D. L., Grimm, R. E., Kaula, W. K., McGill, G. E., Phillips, R. J., Saunders, R. S., Schaber, G., Squyres, S. W., and Stofan, E. R.: 1992, 'Venus Tectonics: An Overview of Magellan Observations', *J. Geophys. Res.* **97**, 13199–13255.

Stofan, E. R., Sharpton, V. L., Schubert, G., Baer, G., Bindschadler, D. L., Janes, D. M., and Squyres, S. W.: 1992, 'Global Distribution and Characteristics of Coronae and Related Features on Venus: Implications for Origin and Relation to Mantle Processes', *J. Geophys. Res.* **97**(E8), 13347–13378.

Strom, R. G.: 1993, 'Parabolic Features and the Erosion Rate on Venus', *Lunar and Planetary Science Conference* **24**, 1371–1372.

Strom, R. G., Schaber, G. G., and Dawson, D. D.: 1994, 'The Global Resurfacing of Venus', *J. Geophys. Res.* **99**, 10899–10926.

Sukhanov, A. L.: 1992, in V. L. Barsukov *et al.* (eds.), *Tesserae, in Venus Geology, Geochemistry, and Geophysics, Research Results from the USSR*, University of Arizona Press, pp. 82-95.

Tanaka, K. L., (compiler): 1994, *Venus Geologic Mappers' Handbook*, Second Edition, U.S. Geological Survey Open File Report 94-438, 50 pp.

Tanaka, K. L. and Scott, D. H.: 1987, *Geological Map of the Polar Regions of Mars*, U.S. Geological Survey Map I-1802-C.

Weitz, C. M., Elachi, C., Moore, H. J., Basilevsky, A. T., Ivanov, B. A., and Schaber, G. G.: 1992, 'Low Emissivity Impact Craters on Venus', *Int. Coll. on Venus, LPI Pub.* **789**, 129–131.

Wilhelms, D. E.: 1972, *Geologic Mapping of the Second Planet*, USGS Interagency Report 55, 36 pp.

Wilhelms, D. E.: 1990, in R. Greeley and R. M. Batson (eds.), *Geologic Mapping, in Planetary Mapping*, Cambridge University Press, New York, pp. 208–260.

Zuber, M. T. and Parmentier, E. M.: 1990, 'On the Relationship between Isostatic Elevation and the Wavelengths of Tectonic Surface Features on Venus', *Icarus* **85**, 290–308.